

APPENDIX A



Characterization of SiC in DLC/a-Si films prepared by pulsed filtered cathodic arc using Raman spectroscopy and XPS

C. Srisang^{a,b,c,*}, P. Asanithi^a, K. Siangchaew^b, A. Pokaipisit^{a,c}, P. Limsuwan^{a,c,*}

^a Department of Physics, Faculty of Science, King Mongkut's University of Technology Thonburi, Bangkok 10140, Thailand

^b Western Digital (Thailand) Company Limited, Ayuthaya 13160, Thailand

^c Thailand Center of Excellence in Physics, CHE, Ministry of Education, Bangkok 10400, Thailand

ARTICLE INFO

Article history:

Received 2 November 2011
Received in revised form 8 February 2012
Accepted 12 February 2012
Available online 19 February 2012

Keywords:

Diamond-like carbon
Amorphous silicon
Silicon carbide
Pulsed filtered cathodic arc

ABSTRACT

DLC/a-Si films were deposited on germanium substrates. a-Si film was initially deposited as a seed layer on the substrate using DC magnetron sputtering. DLC film was then deposited on the a-Si layer via a pulsed filtered cathodic arc (PFCA) system. *In situ* ellipsometry was used to monitor the thicknesses of the growth films, allowing a precise control over the a-Si and DLC thicknesses of 6 and 9 nm, respectively. It was found that carbon atoms implanting on a-Si layer act not only as a carbon source for DLC formation, but also as a source for SiC formation. The Raman peak positions at 796 cm^{-1} and 972 cm^{-1} corresponded to the LO and TO phonon modes of SiC, respectively, were observed. The results were also confirmed using TEM, XPS binding energy and XPS depth profile analysis.

© 2012 Elsevier B.V. All rights reserved.

1. Introduction

Today, the demand for developing high-performance hard coatings has rapidly grown. Among various materials, diamond-like carbon (DLC) becomes a promising material using as a protective coating layer since its hardness approaches that of diamond [1,2]. DLC films are also finding applications as wear and corrosion resistances, anti-reflection and bearing lubricant in various applications, such as hard disk drive, micro-electromechanical system (MEMs), automotive parts, and tools [3–9]. The film can be deposited by various techniques, including microwave plasma [10], ion beam assisted deposition [11], sputter deposition [12], filtered cathodic arc deposition [13], plasma-enhanced chemical vapor deposition [14] and pulsed laser deposition [15]. Although many preparation techniques and many parameters have been extensively studied [16–22], researchers still have problem with low adherence of DLC film on the substrate that may lead to delamination. In order to govern this problem, one of the useful techniques is multilayer coating structures. Castillo et al. reported that the adherence of DLC film on silicon substrate can be improved by adding interface layer, such as amorphous hydrogenated carbon (a-C:H) and titanium nitride (TiN) [23]. Drees et al. supported that using alternating-layered

coatings of Si-DLC/DLC can also enhance wear resistance of the film [24]. Thus, the interface layer between the substrate and DLC film may play an important role. Although there are many reports on improving wear and corrosion resistances and hardness using bi- and multi-layer protective coatings [24–27], the details on the film interface such as a new phase formation has been barely reported.

In this study, amorphous silicon (a-Si) layer with a thickness of 6 nm was sputtered on Ge substrate to perform as the interface layer. DLC film was then deposited on the a-Si layer using a pulsed filtered cathodic arc (PFCA) system. We here reported that, during DLC deposition, carbon atoms implanting on a-Si layer can be able to perform as a source for formation of silicon carbide (SiC) at the DLC/a-Si interface. SiC has long been known for its superior mechanical property, especially for protective coatings [28–30]. The formation of SiC at the interface was confirmed using Raman spectroscopy, transmission electron microscopy (TEM) and X-ray photoelectron spectroscopy (XPS).

2. Experimental details

2.1. Pulsed filtered cathodic arc system

PFCA system used in this work (Veeco, model Nexus DLC-X) is shown by a schematic diagram in Fig. 1. The system consists of four vacuum chambers, i.e. load lock chamber, transfer chamber, pre-clean chamber and PFCA chamber. All chambers were attached together by isolation gate valve. Each has its own turbo molecular pump to evacuate the chamber individually. Ionization gauges were

* Corresponding authors at: Department of Physics, Faculty of Science, King Mongkut's University of Technology Thonburi, Bangkok 10140, Thailand. Tel.: +66 2872 5253; fax: +66 2872 5254.

E-mail address: opticslaser@yahoo.com (P. Limsuwan).

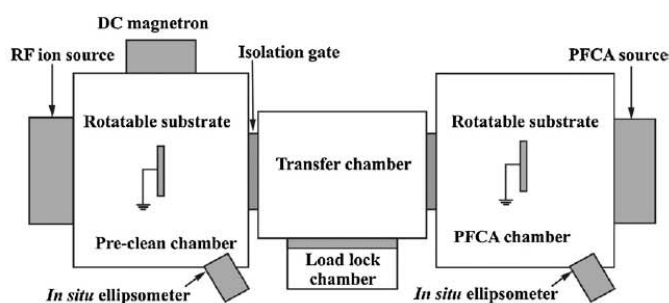


Fig. 1. Schematic diagram of pulsed filtered cathodic arc (PFCA) system.

used to measure the pressure in all four chambers. Prior to the deposition processing of the DLC films, all chambers were evacuated to a base pressure of about 5.0×10^{-7} Torr.

The transfer chamber was equipped with an automated robot arm system for transferring the substrate from load lock chamber to pre-clean and PFCA chambers. The pre-clean chamber was equipped with RF ion source, 16 inch in diameter, and DC magnetron sputtering source with a target of 4 inch in diameter. The ion source was used for pre-cleaning of the substrate whereas the DC magnetron sputtering source was used for the deposition of amorphous silicon (a-Si) as a seed layer. The substrate with deposited silicon layer was then transferred to substrate fixture in the PFCA chamber by robot arm. The PFCA chamber was equipped with a cathodic arc for the deposition of DLC film.

The substrate fixtures in pre-clean and PFCA chambers are capable of tilt and rotation. Therefore, the a-Si seed layer and DLC film can be deposited onto the substrate at any required incident angle. Pre-clean and PFCA chambers were installed with a multi-wavelength ellipsometry (J.A. Woollam, M-2000) for *in situ* monitoring of the film thickness of a-Si layer and DLC film, respectively. Fig. 2 shows a schematic diagram of PFCA chamber and cathodic arc source.

The cathodic arc source includes a high purity graphite cathode of 0.25 inch in diameter and 8 inch in length (99.999% purity),

obtained from Poco Graphite. The arc power supply is operated in pulsed mode. The positive potential of power supply is connected with anode and ground. The voltage between anode and cathode, called arc voltage, can be varied from 0 to 1000V with pulse frequency of 1–5 Hz. Since the distance between anode and graphite cathode is about 2 mm, it is high enough to create current discharge between anode and cathode. Then, graphite is vaporized at the cathode. All charge particles are fed into a curved 90° filter coil [18]. Electrons are moved in spiral along magnetic field generated by filter coil, and ions will be guided due to they are charge particles. In order to improve the film thickness uniformity, a coil operates as a magnetic lens to focus or defocus the plasma beam. A deflection coil is used to raster the beam before striking the substrate. The macro particles move in strange trajectory so they may either leave the filter through openings gap between the turns of the coil or stick to the turns. Thus, unwanted macro particles and neutral atoms are filtered out and coating species reaching the substrate are pure carbon plasma.

2.2. Films preparation

DLC films were deposited using the PFCA deposition method. Crystalline n-type germanium (Ge) wafers with (1 0 0) orientation, and a dimension of 1 cm × 1 cm with a thickness of 0.5 mm were

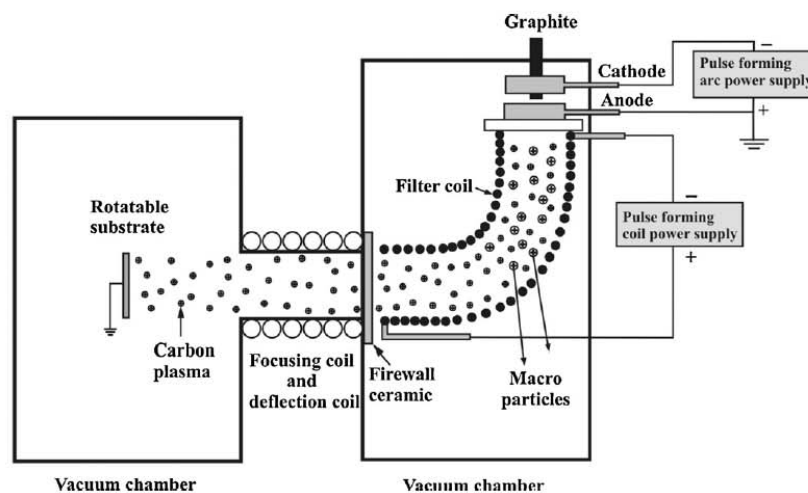


Fig. 2. Schematic diagram of PFCA chamber and cathodic arc source.

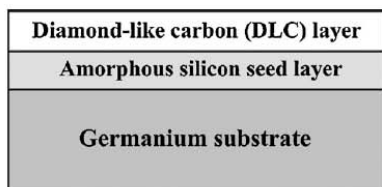


Fig. 3. The layers of DLC film and a-Si layer on germanium substrate.

used as substrates. The DLC deposition process consists of three steps: (1) Ge substrate was cleaned with low energy Ar^+ ion plasma etching at an incident angle of 60° with respect to substrate, for 60 s, (2) a-Si seed layer was deposited on the cleaned germanium substrate at an incident angle of 44° with respect to substrate, using DC magnetron with a power of 150 W and argon gas flow rate of 40 sccm, and (3) DLC layer was deposited at the normal incident angle with respect to substrate using PFCA with a pulse frequency of 1 Hz, arc voltage of 950 V and coil voltage of 900 V. The first two steps were carried out in pre-clean chamber while the third step was done in PFCA chamber. The film thickness was monitored using *in situ* ellipsometry. Fig. 3 shows illustration of deposited films on germanium substrate.

2.3. Characterization

Raman measurements were performed using Renishaw inViaReflex Raman spectrometer with an excitation wavelength of 514 nm from Ar^+ ion gas laser. The laser output is 20 mW and the objective lens is $50\times$. The incident power on the sample is approximately 4 mW. The scan range was from 300 to 1900 cm^{-1} . The XPS depth profiles were recorded by PHI Quantera SXM

scanning X-ray using Al $K\alpha$ X-ray source with a spot size of $200\text{ }\mu\text{m}$. To obtain the depth profile, the DLC/a-Si (9/6 nm) film was etched using ion bombardment from an ion gun of 1 kV for acquiring the XPS spectrum information. The thicknesses of the a-Si layer, SiC layer and DLC films on Ge substrate were investigated using TEM (Tecnai G² 20). Before carrying out TEM cross-sectional image, the DLC/a-Si film was covered with Cr layer which acted as a protective layer to prevent passivation from ion bombardment during cross-section preparation using a focus ion beam (FIB) technique.

3. Results and discussion

The cross-sectional TEM image of DLC/a-Si film in Fig. 4(a) shows that there are three regions of our interest, including a-Si, SiC and DLC. The morphology and density of the film in each region are obviously different as shown in white and gray and are also clearly seen in Fig. 4(b) which is the cropped image of Fig. 4(a) after brightness and contrast adjustment.

In the a-Si region, the morphology of the cross-sectional film is a random structure. The film thickness is slightly less than that of the setting value, 6 nm. Decrease in thickness may be resulted from the depth of maximum carbon implantation into a-Si layer and the formation of a new phase of SiC. Density of a-Si clusters in this region becomes denser toward Ge surface. The difference in the film density may possibly be explained either by the heterogeneous-nucleation behavior of the film itself (i.e. plenty of a-Si structures can be nucleated and formed immediately on Ge surface since it reduces the energy barrier to nucleation of a-Si [31]) or by the out-diffusion of Si atoms due to the SiC nucleation [32]. However, to have better understanding on these phenomena, further experiments may be required.

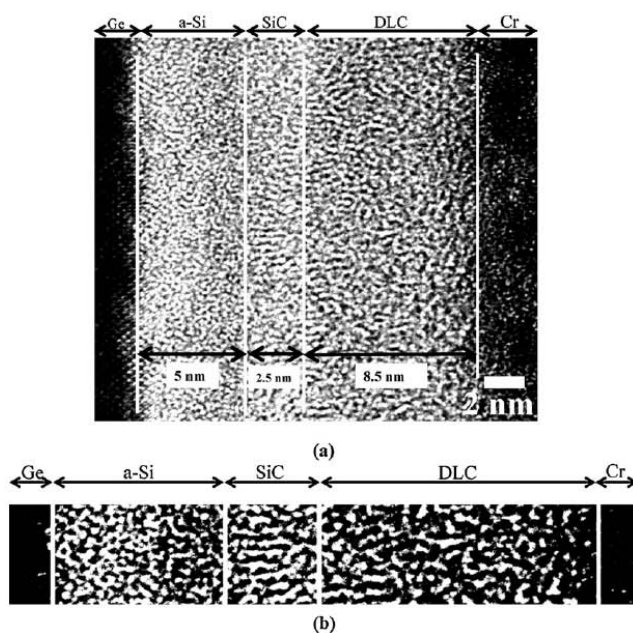


Fig. 4. Cross-sectional TEM image ($\times 1,000,000$) of the films (a) and cropped image from (a) with a brightness and contrast adjustment to provide a clear vision on the cross-sectional morphology of the films (b).

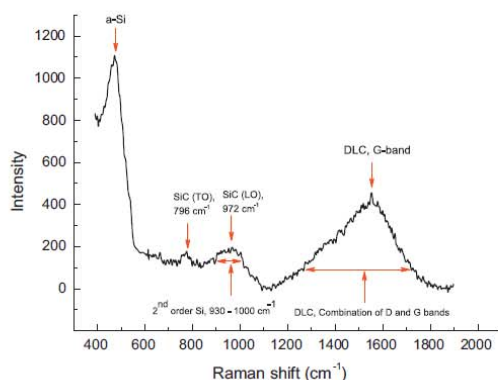


Fig. 5. Raman spectra of DLC/a-Si film with a thickness of 9/6 nm.

Many incoming carbon ions from the source continuously deposit on a-Si layer to form the DLC film. However, the carbons impinging on a-Si layer may act not only as the carbon source for DLC film formation, but also as a source for the SiC formation. At the SiC region, the column-like structure of SiC can be observed as shown in Fig. 4(b), which is in agreement with that observed by Lindner [33]. When carbon atoms transported to a-Si layer, they have enough kinetic energy to penetrate the a-Si layer and chemically react with Si atoms to form SiC to gain a thermodynamic stability. Thickness of this SiC layer is approximately 2.5 nm, which was estimated from the difference in the layer morphology. It should be noted that many factors such as surface roughness of a-Si layer and depth of carbon penetration may result in non-uniform film thickening.

When the flows of carbon atoms are still continued, many of them are not in equilibrium with each other and, hence, react with the neighboring atoms to form DLC structure as shown in the DLC region. The film thickness is approximately 8.5 nm, which is slightly less than that of the setting value, 9 nm, since some of carbon atoms at the a-Si/DLC interface were contributed to the formation of SiC layer. The film morphology was also similar to that of the a-Si layer which is a random structure.

Raman spectroscopy was used to investigate the vibrational modes of carbon and silicon atoms due to chemical bonding, especially in SiC, at the DLC/a-Si interface. The longitudinal optical (LO) and the transversal optical (TO) phonon modes of SiC formation were observed at 796 cm^{-1} and 972 cm^{-1} , respectively, as shown in Fig. 5. The Raman peaks located at these positions are in agreement with those reported for 3C-SiC (β -SiC) [34]. The prominent peak at 480 cm^{-1} is corresponded to the vibrational mode of amorphous Si (a-Si) since it was used as a seed layer for depositing the DLC film [35]. However, no peak from crystalline silicon at 520 cm^{-1} is likely to be observed. This suggests that during the deposition of a-Si layer on germanium substrate there was probably no crystalline silicon formation.

In the higher wavenumber, the broad feature in the 1100–1800 cm^{-1} region is related to the vibrational modes of DLC graphitic characteristics, generally consisting of G and D bands. The maximum peak is corresponded to the G-band locating at about 1554 cm^{-1} , which is different from that of polycrystalline graphite locating at about 1580 cm^{-1} . In general the intensity ratio of G-band to D-band (I_D/I_G) is correlated to the sp^3/sp^2 bonding ratio, representing the physical characteristics of DLC film [36]. Ideally, the value should be close to zero. Thus, by fitting the Raman spectra, the I_D/I_G ratio of DLC film is 0.45. This result confirms that much

Table 1
XPS binding energy of different bonds.

Bond	Binding energy (eV)
C–C	284–284.5
C–Si (C1s)	282.3–283.7
Si–C (Si2p)	99.8–101.3
Si–Si	99.2–99.6

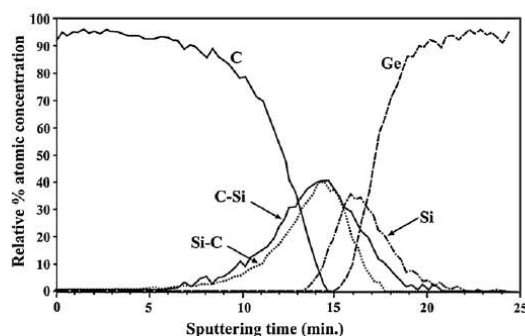


Fig. 6. The XPS depth profile of DLC/a-Si film with a thickness of 9/6 nm on Ge substrate.

more content of the sp^3 of the tetrahedral amorphous carbon (ta-C) structure is presented and it is in agreement with Ferari et al. [37].

To have further qualitative information on SiC formation at the interface, XPS analysis was employed. Table 1 shows binding energies of the chemical bonds found in the DLC/a-Si film (the spectra are not shown). The highest-energy range of 284–284.5 eV is assigned to the bonding of carbon atoms (C–C) in DLC. The C–Si (C1s) and Si–C (Si2p) configurations, corresponding to bonding between carbon and silicon atoms in SiC, are in the ranges of 282.3–283.7 eV and 99.8–101.3 eV, respectively [38]. The lowest energy in the range of 99.2–99.6 eV is stood for the bonding of silicon atoms (Si–Si) in the a-Si layer.

In addition, the XPS sputter depth profile was also carried out to confirm the SiC formation at the DLC/a-Si interface. The DLC/a-Si film with the setting thickness ratio of 9/6 nm was etched using ion bombardment for acquiring the information. The actual depth for each XPS analysis depends upon the etching rate (sputtering time) and the material being etched at any depth. Fig. 6 represents five spectra of the depth profile ranging from DLC film (top layer), SiC layer (C–Si and Si–C), a-Si layer and germanium substrate. At the sputtering time of less than 5 min, the depth profile represents the relative atomic concentration of DLC (C–C) of more than 90%. It gradually decreases for longer sputtering time and becomes 0% at 15 min. The spectra with Gaussian distribution contributed to the SiC (C–Si and Si–C) are initially occurred at about 5 min of sputtering time and becomes maximum at 14 min with the relative atomic concentration of approximately 40%. The presence of these spectra strongly confirmed the SiC formation at the DLC/a-Si interface. The spectrum corresponding to Si–Si bonding of a-Si layer appears at 13 min of sputtering time and reaches the maximum content of 37% at 16 min. The spectrum of Ge substrate begins at 15 min and reaches the maximum value at 18 min. The overlap of the spectra implies the penetration of the atoms during film deposition.

4. Conclusions

We presented that there is a formation of SiC layer at the DLC/a-Si interface during a preparation of DLC/a-Si bilayer film

on germanium substrate. Carbon atoms impinging on a-Si layer act not only as a carbon source for DLC formation, but also as a source for SiC formation. The result was clearly observed by TEM image representing a 2.5 nm layer of SiC. The LO and TO phonon modes of SiC were presented at the Raman peaks of 796 cm^{-1} and 972 cm^{-1} , respectively, indicating 3C–SiC (B–SiC) structure. The results were also confirmed using XPS binding energy and XPS depth profile analysis. Scratch testing of the DLC film shows that at the critical load of $58\text{ }\mu\text{N}$ the film fails in the penetration depth of 19.5 nm . This is a good adhesion compared with 10 nm thick DLC film reported by Hysitron Incorporated [39] which is failed at $32\text{ }\mu\text{N}$. The observation may shed light on many potential applications, especially in protective coatings such as hard disk drive, MEMs, automotive parts, tools and devices since the SiC formation may be able to improve DLC/a-Si adhesive strength, hardness and wear resistance.

Acknowledgments

This work was supported by Industry/University Cooperative Research Center (I/UCRC) in HDD Advanced Manufacturing, Institute of Field Robotics, King Mongkut's University of Technology Thonburi and National Electronics and Computer Technology Center, National Science and Technology Development Agency. This work was partially supported by Thailand Center of Excellence in Physics (ThEP) and King Mongkut's University of Technology Thonburi under The National Research University Project.

References

- [1] M.V. Gadowski, A.C. Ferrari, R. Ohr, B. Jacoby, H. Hilgers, H.H. Schneider, H. Adrian, *Surf. Coat. Technol.* 174–175 (2003) 246.
- [2] J. Robertson, *Mater. Sci. Eng. R* 37 (2002) 129.
- [3] J. Robertson, *Thin Solid Films* 383 (2001) 81.
- [4] M.G. Beghi, A.C. Ferrari, K.B.K. Teo, J. Robertson, C.E. Bottani, A. Libassi, B.K. Tanner, *Appl. Phys. Lett.* 81 (2002) 3804.
- [5] H. Kohira, V. Prabhakaran, F.E. Talke, *Tribol. Int.* 33 (2000) 315.
- [6] W.C. Poh, S.N. Piramanayagam, J.R. Shi, T. Liew, *Diamond Relat. Mater.* 16 (2007) 379.
- [7] B. Tomcik, T. Osipowicz, J.Y. Lee, *Thin Solid Films* 360 (2000) 173.
- [8] M. Kano, *New Diamond Front. Carbon Technol.* 16 (2006) 201.
- [9] S.A. Smallwood, K.C. Eapen, S.T. Patton, J.S. Zabinski, *Wear* 260 (2006) 1179.
- [10] D.S. Patil, K. Ramachandran, N. Venkatramani, M. Pandey, R.D. Cunha, *Pramana J. Phys.* 55 (2000) 933.
- [11] C. Weissmantel, K. Bewilogua, D. Dietrich, H.J. Erler, H.J. Hinneberg, S. Klose, W. Nowick, G. Reisse, *Thin Solid Films* 72 (1980) 19.
- [12] N. Savvides, *J. Appl. Phys.* 59 (1986) 4133.
- [13] S. Xu, B.K. Tay, H.S. Tan, Li Zhong, Y.Q. Tu, S.R.P. Silva, W.I. Milne, *J. Appl. Phys.* 79 (1996) 7234.
- [14] J.Y. Shim, E.J. Chi, H.K. Baik, S.M. Lee, *Jpn. J. Appl. Phys.* 37 (1998) 440.
- [15] H.S. Scheibe, D. Drescher, B. Schultrich, M. Falz, G. Leonhardt, R. Wilberg, *Surf. Coat. Technol.* 85 (1996) 209.
- [16] F.X. Liu, K.L. Yao, Z.L. Liu, *Diamond Relat. Mater.* 16 (2007) 1746.
- [17] F.X. Liu, Z.L. Wang, *Surf. Coat. Technol.* 203 (2009) 1829.
- [18] W. Zhanga, A. Tanakab, K. Wazumia, Y. Kogab, *Diamond Relat. Mater.* 11 (2002) 1837.
- [19] D. Sheeja, B.K. Tay, S.P. Lau, Xu Shi, *Wear* 249 (2001) 433.
- [20] M. Maharizi, O. Segal, E. Jacob, Y. Rosenwaks, T. Meoded, N. Croitoru, A. Seidman, *Diamond Relat. Mater.* 8 (1999) 1050.
- [21] M. Zhong, C. Zhang, J. Luo, *Appl. Surf. Sci.* 254 (2008) 6742.
- [22] J. Jiang, R.D. Arnell, *Wear* 239 (2000) 1.
- [23] H.A. Castillo, E.R. Parra, P.J. Arango, *Appl. Surf. Sci.* 257 (2011) 2665.
- [24] D. Drees, J.P. Celis, E. Dekempeneer, J. Meneve, *Surf. Coat. Technol.* 86–87 (1996) 575.
- [25] J.W. Yi, J. Kim, M. Moon, K. Lee, S. Kim, *Tribol. Lett.* 34 (2009) 223.
- [26] A.A. Voevodin, S.D. Walck, J.S. Zabinski, *Wear* 203–204 (1997) 516.
- [27] M.P. Delplancke-Ogletree, O.R. Monteiro, *Surf. Coat. Technol.* 108–109 (1998) 484.
- [28] S. Mahdavi, F. Akhlaghi, *J. Mater. Sci.* 46 (2011) 7883.
- [29] Y. Zhan, G. Zhang, *J. Mater. Sci. Lett.* 22 (2003) 1087.
- [30] M. Gui, S.B. Kang, *Metall. Mater. Trans. A* 32A (2004) 2383.
- [31] T. Brar, P. France, P.G. Smirniotis, *J. Phys. Chem. B* 105 (2001) 5383.
- [32] I.S. Moon, G. Cho, *Mater. Sci. Eng. C* 24 (2004) 301.
- [33] J.K.N. Linder, *Appl. Phys. A* 77 (2003) 27.
- [34] C.J. Lee, G. Pezzotti, Y. Okui, S. Nishino, *Appl. Surf. Sci.* 228 (2004) 10.
- [35] M. Veres, M. Koós, S. Tóth, M. Füle, I. Pöcsik, A. Tóth, M. Mohai, I. Bertóti, *Diamond Relat. Mater.* 14 (2005) 1051.
- [36] A.C. Ferrari, J. Robertson, *Phys. Rev. B* 61 (2000) 14095.
- [37] A.C. Ferrari, A. Libassi, B.K. Tanner, V. Stolojan, J. Yuan, L.M. Brown, S.E. Rodil, B. Kleinsorge, J. Robertson, *Phys. Rev. B* 62 (2000) 11089.
- [38] W. Cho, Y. Oh, C. Kim, M. Osada, M. Kakhana, D. Lim, D. Cheong, *J. Alloys Compd.* 285 (1999) 255.
- [39] M. Dickinson, Application Note Nanoindentation of DLC Coatings, www.hysitron.com.

APPENDIX B

Slider Curvature Control Through Dicing Process

Chirawat Srisang^{1,2,3,a}, Krisda Siangchaew^{2,b}, Jakrapong Kaewkhao^{3,4,c},
 Artorn Pokaipisit^{1,3,d} and Pichet Limsuwan^{1,3,e}

¹Department of Physics, Faculty of Science, King Mongkut's University of Technology Thonburi,
 Bangkok 10140, Thailand

²Western Digital (Thailand) Company Limited, Ayuthaya 13160, Thailand

³Thailand Center of Excellence in Physics, CHE, Ministry of Education,
 Bangkok 10400, Thailand

⁴Center of Excellence in Glass Technology and Materials Science (CEGM),
 Nakhon Pathom Rajabhat University, Nakhon Pathom 73000, Thailand

^aJirawat.Srisung@wdc.com, ^bopticslaser@yahoo.com, ^cmink110@hotmail.com,
^dpokaipisit@gmail.com, ^epichet.lim@kmutt.ac.th

Keywords: Air bearing surface, Camber, Crown, Dicing Process.

Abstract. In the manufacturing of slider, the final step is a dicing process of the rowbars into individual slider. However, in all slider separation processes seem to affect the curvature of the slider air bearing surface (ABS). As a result, the change in ABS crown and camber which can significantly affect the fly height of the slider. This paper investigates the influence of three types of dicing process, with the same feed rate and cutting speed, on the ABS curvature.

Introduction

Currently, the areal storage density in hard disk drives is rapidly increasing with the reducing of the slider flying height. The slider flying height in modern disk drives is typically 10 nm and continues to reduce which result in an increasing of the read signals. The curvature control of the slider air bearing surface (ABS) is a critical method for flying height control during the slider fabrication process. It is well-known that a few nanometers change in the crown can significantly affect the fly height of the slider. The camber also affects the tribological behavior of the slider on the rotating disk, during start/stop or slider load/unload operations [1,2]. Hence, it is necessary to control the crown and camber during the slider fabrication process. In recent years, several technologies have been used for the curvature adjustment of the slider ABS, such as spherically curved lapping plate, grinding, diamond-tip scribing, laser scribing [3,4], lapping, inductive couple plasma etching [5], and other trade secret methods.

In this paper, three types of dicing process for slider separation were investigated. The change on ABS curvature was characterized using phase shifting and vertical scanning interferometry.

Theory

Fig. 1(a) illustrates a slider with an ABS curvature profile pattern and various slider curvature parameters that are important for flying height control.

Camber is defined as the maximum separation of the cross curvature from the imaginary plane drawn between two side edges of the slider (Fig. 1(b))

Crown is defined as the maximum separation of the cylindrical contour along the length (y-axis) from the plane drawn between leading and trailing edges of the ABS. (Fig. 1(c))

Fly height is a distance between the magnetic elements and the magnetic surface. Current technology requires that the fly height is lower than 0.4 micro-inch. All the slider curvature parameters shown in Fig. 1 are in the order of nanometer, so the drawing in Fig. 1 is greatly exaggerated.

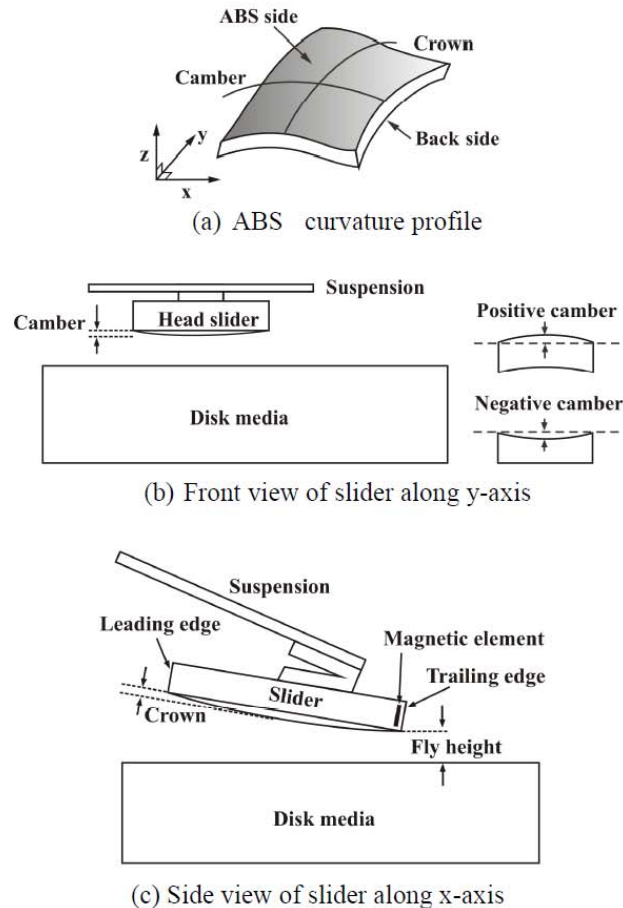


Fig. 1 (a) Showing ABS curvature profile, (b) front view of slider showing the camber and (c) side view of slider showing the crown and fly height.

Experimental, results and discussion

A. Slider fabrication. The material used in this study is the round wafer of 6 inch in diameter manufactured by Neo Max and the trade name is AC72F. It is a composite ceramics material consisting of Al_2O_3 -TiC (known to industry as AlTiC). Its physical properties are as follows: density $4,300 \text{ kg/m}^3$, Poisson's ratio 0.22, Young's modulus 390 GPa, specific heat $880 \text{ J/kg } ^\circ\text{C}$, thermal conductivity $6,302 \text{ W/m}^\circ\text{C}$ and resistivity $20,000 \text{ } \Omega\text{-m}$.

The process starts from wafer polishing for bow correction. Then, metal hard coating was performed using sputtering technique. Thereafter, the ABS patterning on metal mask was carried out and unwanted metal mask on exposed area was chemically etched. Finally, the ABS pattern was dry etched utilizing reactive ion etching (RIE) for cavity step.

The wafer was scribed for wing patterning and sliced into rowbars, each with a dimension of $1.29 \text{ mm} \times 49.54 \text{ mm} \times 0.43 \text{ mm}$ precision lapping operation was then performed on the individual rowbar to produce desire ABS profile subsequently, the ABS was coated with diamond-like carbon (DLC) for surface protection. The final process is the dicing process of the rowbars into individual slider of dimension $1.29 \text{ mm} \times 1.73 \text{ mm} \times 0.43 \text{ mm}$. In this study, the designed dimension of individual slider is shown in Fig. 2

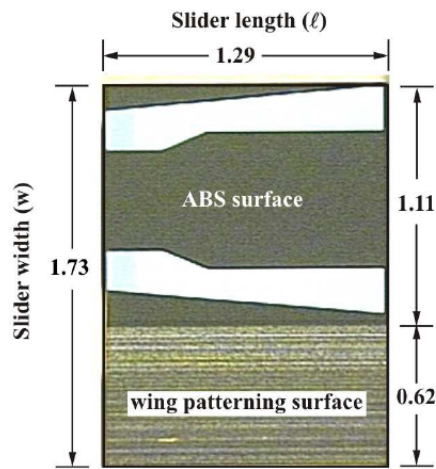


Fig. 2 Showing dimension, ABS surface and wing patterning surface.

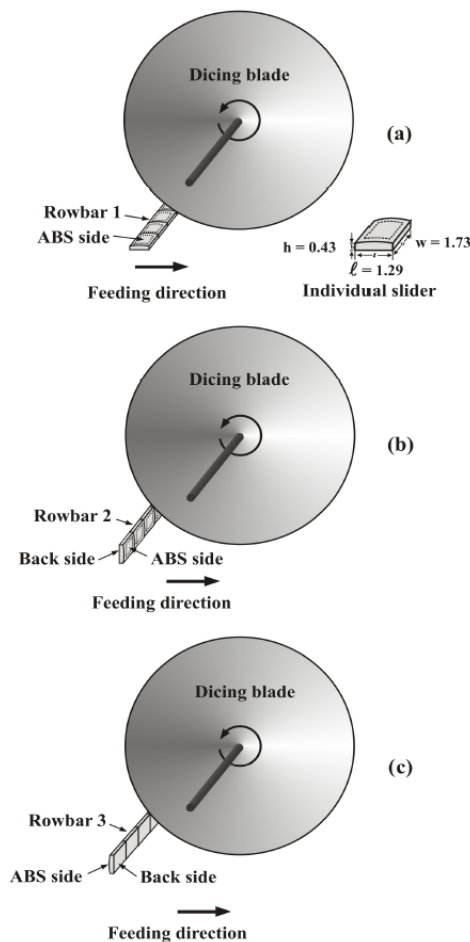


Fig. 3 Schematic diagram for three types of dicing process

It is seen that the slider width (1.73 mm) is longer than the slider length (1.29 mm). Because in this design, part of the slider width (0.62 mm) was scribed for wing patterning. This part was used for the attachment of a sensor to detect the media asperity during the slider flying over the media surface. Therefore, each rowbar can be diced into 27 sliders, each with a dimension (length \times width \times thickness) of 1.29 mm \times 1.73 mm \times 0.43 mm.

B. Dicing process. The diamond blade with a diameter of 110 mm and 110 μ m thick was used for dicing the rowbars. The rotational blade velocity is 9,000 rpm. The rowbar was fed to the blade at a rate of 3 inch/min. A water based coolant with a flow rate of 2 gal/min was dispensed onto the blade and substrate interface. In this work, the above cutting parameters were kept constant for all experiments. dicing process.

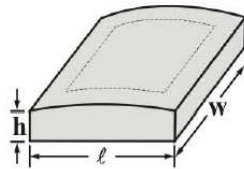
Three types of dicing process were used in the experiment as shown in Fig. 3. In Fig. 3(a), the ABS surface is faced up and moved to the dicing blade. In Figs. 3(b) and 3(c) the ABS side and the back side are moved to the dicing blade, respectively. Each type of dicing process, one rowbar was diced and hence 27 sliders were obtained.

C. ABS surface characterization. The ABS 3-D surface profile measurements were performed using phase-shifting and vertical scanning interferometry (Wyko HD8100). He-Ne laser that emits the light at a wavelength of 632.8 nm together with a filter of bandwidth 3 nm was used as the light source. This technique is a non-contact surface topography via fitted model of an elliptical paraboloid. The camber and crown for ABS surface were then obtained. In present work, the ABS surface of slider rowbars before and after dicing was characterized and the results on the camber and camber change (i.e. the change of camber value after dicing) are shown in Table 1. It is noted that the crown change is very small for all three rowbars, therefore it is not reported here.

It is seen from Table 1 that the average value of the camber change for rowbars 1-3 are -0.76, -1.58 and 1.70 nm, respectively. The minimum and maximum of camber change were obtained from the dicing process corresponding to Fig. 3(a) and Fig. 3(c), respectively. Furthermore, negative cambers were induced in rowbar 1 (Fig. 3(a)) and rowbar 2 (Fig. 3(b)), whereas positive camber was induced in rowbar 3 (Fig. 3(c)) as we expected.

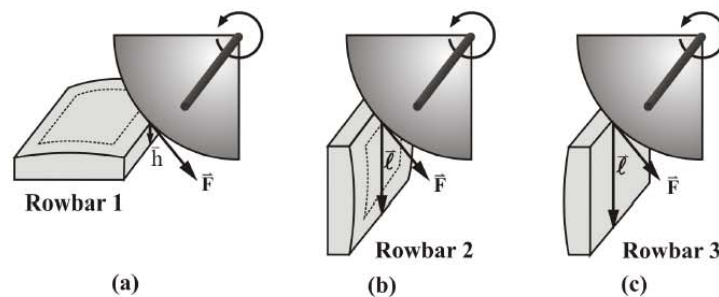
Table 1 The camber values for rowbar1-3 obtained from three types of dicing process.

Slider Number	Rowbar 1			Rowbar 2			Rowbar 3		
	Before Dicing (nm)	After Dicing (nm)	Delta (nm)	Before Dicing (nm)	After Dicing (nm)	Delta (nm)	Before Dicing (nm)	After Dicing (nm)	Delta (nm)
1	1.97	1.02	-0.95	3.58	1.89	-1.69	2.34	4.16	1.82
2	0.49	-0.36	-0.85	2.45	0.74	-1.71	1.81	3.63	1.82
3	1.47	0.57	-0.89	0.83	-0.82	-1.65	1.54	3.30	1.76
4	-1.94	-2.72	-0.78	0.66	-0.98	-1.64	1.89	3.68	1.79
5	0.07	-0.62	-0.69	0.17	-1.40	-1.56	-1.08	0.65	1.73
6	-0.65	-1.33	-0.69	-0.02	-1.51	-1.50	0.29	2.02	1.74
7	0.58	-0.24	-0.82	-0.65	-2.17	-1.52	-0.76	0.85	1.61
8	-0.43	-1.20	-0.77	-0.22	-1.66	-1.44	0.97	2.62	1.65
9	-0.16	-0.88	-0.72	-1.20	-2.77	-1.57	1.15	2.84	1.69
10	0.50	-0.23	-0.72	0.73	-0.90	-1.63	-0.58	1.04	1.63
11	-1.43	-2.15	-0.72	-3.48	-4.89	-1.42	0.25	1.91	1.66
12	-0.31	-1.08	-0.76	-1.46	-2.98	-1.53	-2.27	-0.71	1.56
13	-0.95	-1.70	-0.75	0.24	-1.40	-1.63	-2.34	-0.72	1.63
14	-0.06	-0.73	-0.67	1.51	-0.12	-1.63	-0.77	0.92	1.69
15	0.16	-0.50	-0.66	0.07	-1.52	-1.59	-0.10	1.52	1.62
16	1.04	0.41	-0.63	-1.14	-2.69	-1.55	0.12	1.72	1.61
17	0.26	-0.42	-0.68	-1.44	-2.90	-1.47	-0.03	1.62	1.65
18	0.20	-0.38	-0.58	-0.18	-1.71	-1.53	-0.98	0.62	1.61
19	-1.50	-2.16	-0.67	1.18	-0.43	-1.61	1.65	3.34	1.68
20	-1.72	-2.51	-0.79	0.38	-2.03	-1.65	0.23	1.86	1.63
21	-1.16	-1.83	-0.66	-1.23	-2.72	-1.48	-2.32	-0.63	1.69
22	1.09	0.32	-0.77	-0.90	-2.60	-1.69	-0.21	1.57	1.78
23	-0.60	-1.42	-0.81	-0.55	-1.94	-1.39	0.16	1.84	1.68
24	0.58	-0.31	-0.89	0.10	-1.58	-1.67	-1.87	-0.21	1.66
25	1.72	0.90	-0.82	1.08	-0.58	-1.66	0.84	2.60	1.76
26	1.72	0.93	-0.79	1.79	0.12	-1.67	1.31	3.16	1.85
27	2.23	1.29	-0.95	2.68	0.97	-1.71	1.96	3.84	1.87
Average	0.12	-0.64	-0.76	0.16	-1.43	-1.58	0.12	1.82	1.70

Fig. 4 Dimension of each slider is $\ell \times w \times h$.

As stated earlier that the camber change results in the stress induced in ABS surface. The stress induced in ABS surface due to dicing processes in Fig. 3 can be explained in terms of cutting force (\bar{F}) and torque ($\bar{\tau}$)

If the dimension of each slider shown in Fig. 4 is $\ell \times w \times h$ (where $w > \ell > h$). Therefore, the cutting force and cutting rowbar surface of three dicing processes corresponding to Fig. 3 (a)-(c) can be drawn as shown in Fig. 5 (a)-(c), respectively.

Fig. 5 Diagram showing the vectors of cutting force \bar{F} , the thickness \bar{h} and the length $\bar{\ell}$.

During cutting, the torque induced in Fig. 5 (a)-(c) are $\bar{h} \times \bar{F}$, $< \bar{\ell} \times \bar{F}$ and $\bar{\ell} \times \bar{F}$, respectively. It is seen that the lowest torque, $\bar{h} \times \bar{F}$, is obtained from the dicing process in Fig. 3(a) and highest torque, $\bar{\ell} \times \bar{F}$, is obtained from the dicing process in Fig. 3 (c). This conclusion is in good agreement with the result on the camber change as shown in Table 1.

Summary

The slider dicing process, the final machining process of slider fabrication, will affect the curvature of the slider air bearing surface the (ABS). The stress induced in the ABS surface contributes to the ABS crown and camber which significantly affect the fly height of the slider. Three types of dicing process depend on the rowbar configuration and cutting direction were investigated.

Acknowledgments

This work was supported by Industry/University Cooperative Research Center (I/UCRC) in HDD Advanced Manufacturing, Institute of Field roBOTics, King Mongkut's University of Technology Thonburi and National Electronics and Computer Technology Center, National Science and Technology Development Agency. This work was also supported by KMUTT under the National Research University project.

References

- [1] M. Suk, T. Ishii and D. Bogy: Trans. ASME Vol. 114 (1992), p. 26
- [2] J.J.K. Lee, J. Enguero, M. Smallen, A. Chao and E. Cha: Trans. ASME Vol. 117 (1995), p. 350
- [3] A.C. Tam, C.C. Poon, L. Crawforth and P.M. Lundquist: Data Storage (1999), p. 29
- [4] A.C. Tam, C.C. Poon and L. Crawforth: Analyt. Sci. Vol. 17 (2001), p. 419
- [5] M. Zhang, Y.S. Hor, G. Han and B. Liu: IEEE Trans. Magn. Vol. 38 (2002), p. 2162.

APPENDIX C

Research Article

Raman Spectroscopy of DLC/a-Si Bilayer Film Prepared by Pulsed Filtered Cathodic Arc

C. Srisang,^{1,2,3} P. Asanithi,¹ K. Siangchaew,² S. Limsuwan,¹
A. Pokaipisit,^{1,3} and P. Limsuwan^{1,3}

¹Department of Physics, Faculty of Science, King Mongkut's University of Technology Thonburi, Bangkok 10140, Thailand

²Western Digital (Thailand) Company Limited, Ayuthaya 13160, Thailand

³Thailand Center of Excellence in Physics, CHE, Ministry of Education, Bangkok 10400, Thailand

Correspondence should be addressed to A. Pokaipisit, pokaipisit@gmail.com

Received 1 August 2012; Revised 4 October 2012; Accepted 4 October 2012

Academic Editor: Sheng-Rui Jian

Copyright © 2012 C. Srisang et al. This is an open access article distributed under the Creative Commons Attribution License, which permits unrestricted use, distribution, and reproduction in any medium, provided the original work is properly cited.

DLC/a-Si bilayer film was deposited on germanium substrate. The a-Si layer, a seed layer, was firstly deposited on the substrate using DC magnetron sputtering and DLC layer was then deposited on the a-Si layer using pulsed filtered cathodic arc method. The bilayer films were deposited with different DLC/a-Si thickness ratios, including 2/2, 2/6, 4/4, 6/2, and 9/6. The effect of DLC/a-Si thickness ratios on the sp^3 content of DLC was analyzed by Raman spectroscopy. The results show that a-Si layer has no effect on the structure of DLC film. Furthermore, the upper shift in G wavenumber and the decrease in I_D/I_G inform that sp^3 content of the film is directly proportional to DLC thickness. The plot modified from the three-stage model informed that the structural characteristics of DLC/a-Si bilayer films are located close to the tetrahedral amorphous carbon. This information may be important for analyzing and developing bilayer protective films for future hard disk drive.

1. Introduction

In current hard disk drive technology, data are written and retrieved by a magnetic recording head, which consists of a magnetic transducer and a sensor, flying over the disk surface at a height of 10 nm or lower. At this tiny space, problems may occur if the recording head contacts with the disk surface during operation. Thus, coating recording head and disk surface with a protective film is highly required as it will minimize the contact force at the head/disk interface. At present, DLC film is becoming a preferred coating for the head and disk surface because of their unique properties of the sp^3 structure that is similar to the physical properties of diamond, such as high density, high wear resistance, low friction coefficient, chemical inertness, and optical transparency [1–6].

DLC film can be prepared by various methods, for example, ion beam assisted deposition [8], sputtering [9], filtered cathodic arc [10], plasma-assisted chemical vapor deposition [11], and pulsed laser deposition [12]. However, different preparation methods may offer DLC film of different forms,

such as hydrogenated form of amorphous carbon (a-C:H) and nonhydrogenated form called tetrahedral amorphous carbon (ta-C). Most of the a-C:H form contains sp^3 fractions of less than 50%, while the ta-C can contain sp^3 fractions of up to 85% [13, 14]. Thus, the preferred structure of DLC for being a protective film is the tetrahedral amorphous carbon (ta-C). Liu and Wang [3], and Liu et al. [15] reported the coating of Si layer with a thickness of 1 nm on the substrate as seed layer before coating DLC film. However, the effects of Si layer on the sp^3 content of DLC film were not discussed.

In this work, amorphous silicon (a-Si) layer was initially deposited on germanium (Ge) substrate using direct current (DC) magnetron sputtering. Diamond-like carbon (DLC) layer was then deposited on the a-Si layer using pulsed filter cathodic arc (PFCA). The effects of a-Si layer thickness on the sp^3 content of DLC film were studied by varying the thicknesses of a-Si and DLC layers from 2 to 6 nm and 2 to 9 nm, respectively, depending on the DLC/a-Si thickness ratios, including 2/2, 2/6, 4/4, 6/2, and 9/6. Therefore, the total thicknesses of DLC/a-Si films are 4, 8, 8, 8, and 15 nm, respectively. The sp^3 content of DLC/a-Si films

were characterized by Raman spectroscopy and transmission electron microscopy (TEM).

2. Experimental

DLC/a-Si bilayer films were deposited using the pulsed filtered cathodic arc (PFCA) system. The system consists of four vacuum chambers, including (i) load lock chamber, (ii) transfer chamber, (iii) preclean chamber, and (iv) pulsed filtered cathodic arc (PFCA) chamber. Crystalline n-type germanium wafers with (100) orientation, and a dimension of $1 \times 1 \text{ cm}^2$ with a thickness of 0.05 cm were used as a substrate. The DLC/a-Si deposition process consists of three steps: (i) the substrate was cleaned with low energy Ar^+ ion plasma etching at an incident angle of 60° with respect to substrate, for 60 sec, (ii) a-Si seed layer was deposited on the Ge substrate at an incident angle of 44° with respect to the substrate, using DC magnetron with a power of 150 W and an argon gas flow rate of 40 sccm, and (iii) DLC layer was deposited at the normal incident angle with respect to the substrate using pulsed filtered cathodic arc (PFCA) with a pulse frequency of 1 Hz, arc voltage of 950 V, and coil voltage of 900 V. The first two steps were carried out in preclean chamber, while the third step was prepared in the PFCA chamber. The film thickness was monitored using *in situ* ellipsometry. Table 1 shows the details of the DLC/a-Si thickness ratios for all DLC/a-Si films.

Thickness of DLC/a-Si film on Ge substrate was investigated using TEM (Tecnai G2 20). It should be noted that before carrying out TEM cross-sectional image, the DLC/a-Si film was coated with Cr layer. This additional layer acts as a protective layer to prevent passivation from ion bombardment during cross-sectional preparation using a focused ion beam (FIB). Raman measurements were performed with a Renishaw inVia Reflex Raman Spectrometer at 514 nm of Ar^+ ion gas laser. The laser output power of 20 mW and 50x objective lens were used, which resulted in an incident power at the sample of approximately 4 mW. The scan range was from 1180 to 1800 cm^{-1} . The raw spectra were fitted using Gaussian profile to obtain smooth curve. Then, the smooth curve was fitted with two Gaussian-Lorentzian functions corresponding to the G and D band wavenumbers. G band is originated from the stretching vibration of any pair of sp^2 sites, whether in C=C chains or in hexagonal rings, while D band is the breathing mode of those sp^2 sites only in rings, not in chains [7, 14].

3. Results and Discussion

Cross-sectional morphologies of DLC/a-Si films prepared from different DLC/a-Si thickness ratios (2/2, 2/6, 4/4, 6/2, and 9/6) are similar, but they are different in the thickness of a-Si and DLC layers. Figure 1(a) shows a typical cross-sectional TEM image of the bilayer film prepared from the DLC/a-Si thickness ratio of 9/6 on Ge substrate. There are four regions presented in the image, including Ge substrate, a-Si layer, DLC layer, and Cr layer (a protective layer for preventing passivation from ion bombardment during

TABLE 1: Thickness of DLC and a-Si layers, DLC/a-Si thickness ratio, and total thickness of DLC/a-Si film.

DLC layer (nm)	Thickness		Total thickness (nm)
	a-Si layer (nm)	DLC/a-Si Thickness ratio	
2	2	2/2	4
2	6	2/6	8
4	4	4/4	8
6	2	6/2	8
9	6	9/6	15

TABLE 2: Information extracted from Raman spectra of DLC/a-Si films prepared from different DLC/a-Si thickness ratios.

DLC/a-Si thickness ratio	Total thickness (nm)	G Wavenumber (cm^{-1})	I_D/I_G
2/2	4	1552	1.528
2/6	8	1552	1.507
4/4	8	1557	0.744
6/2	8	1561	0.568
9/6	15	1565	0.453

preparation of cross-sectional film). Two regions according to a-Si and DLC layers are of our interest. The morphology and density of a-Si and DLC layers are slightly different as shown in white and gray and are also seen in Figure 1(b) which is the cropped image of Figure 1(a) after brightness and contrast adjustment.

The structural characteristics of DLC layer prepared from different DLC/a-Si thickness ratios were investigated by Raman spectroscopy. Figure 2 shows Raman spectra of DLC/a-Si films prepared from the DLC/a-Si thickness ratios of 2/2, 2/6, 4/4, 6/2, and 9/6. The spectra exhibit a broad wavenumber ranging from 1200 to 1800 cm^{-1} . This informs the formation of sp^2 and sp^3 contents, which can be used for indicating the structural characteristics of DLC layer [16].

To have further understanding on the structural characteristics of the bilayer film, Raman spectrum of DLC/a-Si film from each thickness ratio was fitted to obtain G-band wavenumber and D/G intensity ratio (I_D/I_G) using Gaussian function. The typical fitted spectrum of DLC/a-Si film is shown in Figure 3 which includes graphite (G) band, disorder (D) band, and fitted spectrum. G-band wavenumber and I_D/I_G ratio from the fitted spectra are given in Table 2. For DLC/a-Si ratios of 2/2 and 2/6, where DLC film thickness is 2 nm and a-Si layer thicknesses are 2 and 6 nm, respectively. The G band positions for these two ratios are the same with a G wavenumber of 1552 cm^{-1} . This result indicates that a-Si layer has no effect on the structure of ta-C film. For DLC/a-Si ratios of 4/4, 6/2, and 9/6, that is the thicknesses of DLC film are 4, 6, and 9 nm, respectively. It is seen from Table 2 that the G band position shifts to the higher wavenumber when the thickness of DLC film increases. This result implies that the structure of ta-C film depends only on the thickness of DLC film. The thicker DLC layer in the bilayer film offers higher vibrational energy which comes

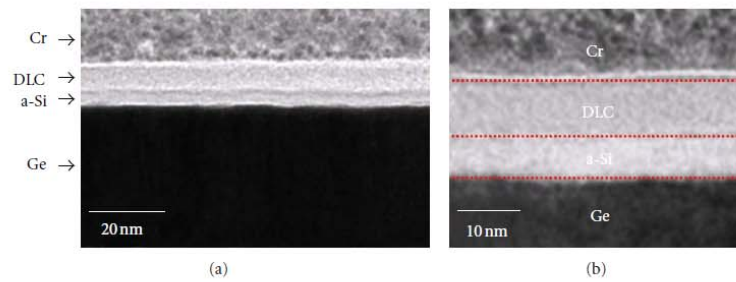


FIGURE 1: (a) Cross-sectional TEM image of the bilayer film prepared from the DLC/a-Si thickness ratio of 9/6. (b) Cropped image from (a) with a brightness and contrast adjustment to provide a clear vision on the cross-sectional morphology of the films.

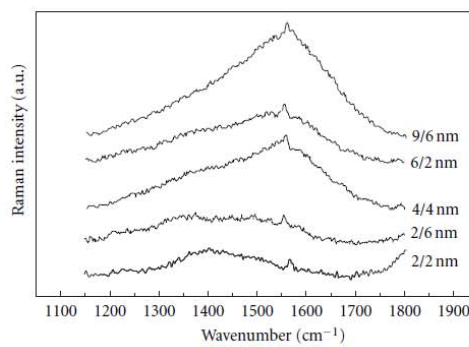


FIGURE 2: Raman spectra of the bilayer films prepared from different DLC/a-Si thickness ratios: 2/2, 2/6, 4/4, 6/2, and 9/6.

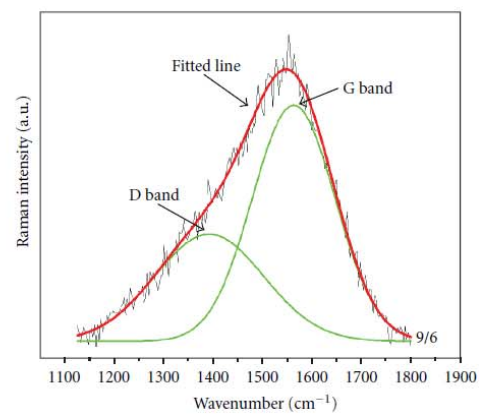


FIGURE 3: Raman spectrum of the bilayer film was fitted into G and D bands. The film was prepared from the DLC/a-Si thickness ratio of 9/6.

from the change in bond stretching mechanism of any pair of sp^2 sites due to the increase in short $\text{C}=\text{C}$ chain contents [7, 17] and result in the higher sp^3 contents of ta-C structure [14, 18, 19].

This result is also in agreement with the three-stage model reported by Ferrari and Robertson [7] to analyze Raman spectra of ta-C film. As shown in Figure 4, the relationship between G-band wavenumber of DLC/a-Si film and its thickness ratios was plotted. The data analyzed according to the three-stage model inform that G-band wavenumber can be used for indicating sp^2 configuration of the material. For example, the G-band wavenumbers at 1580, 1600, 1510, and 1570 cm^{-1} indicate the sp^2 site from graphite, nanocrystalline-graphite (NC-graphite), amorphous carbon (a-C), and tetrahedral amorphous carbon (ta-C), respectively. Thus, Figure 4 confirms that the structural characteristics of DLC layers prepared from all types of DLC/a-Si thickness ratio are very close to the tetrahedral amorphous carbon (ta-C) structure since they are located close to the ta-C structure.

To confirm the previous explanation on the sp^3 content, the I_D/I_G ratio which is normally correlated to the sp^3/sp^2 fraction was evaluated. Ideally, the I_D/I_G value for ta-C should be close to zero since the D band is the breathing

mode of sp^2 sites only in rings, not in chains [7]. The I_D/I_G ratios of DLC/a-Si films are 1.528, 0.568, and 0.453 for the DLC/a-Si thickness ratios of 2/2, 6/2, and 9/6, respectively, as shown in Figure 5. This result indicates that when DLC layer becomes thicker, there are more sp^3 contents. Moreover, from the plot in Figures 4, and 5, it was found that the thickness of a-Si layer has no effect on the DLC formation and the sp^3/sp^2 fraction. However, it may have an important role in the mechanical properties of the DLC film such as adhesion, hardness, and wear resistance which will be necessary for future investigation.

4. Conclusions

DLC/a-Si bilayer films of different DLC/a-Si thickness ratios were deposited on Ge substrates. G-band wavenumber shifts to higher value when the thickness of DLC layer increases due to higher sp^3 contents. This is also confirmed by the decrease in I_D/I_G ratio. The plot modified from the three-stage model points out that the structural characteristics of DLC layers

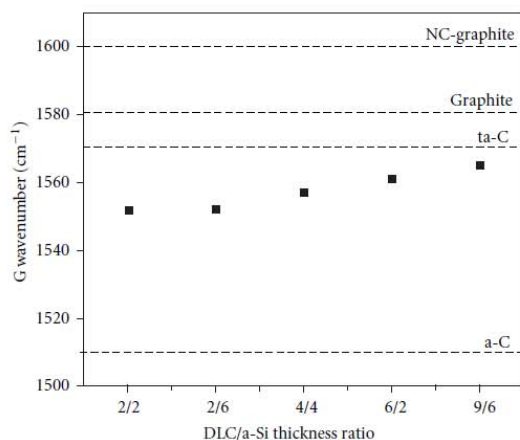


FIGURE 4: The plot modified from the three-stage model [7] to obtain structural characteristics of DLC in the bilayer film. Four structures are presented: nanocrystalline-graphite (NC-graphite), graphite, amorphous carbon (a-C), and tetrahedral amorphous carbon (ta-C).

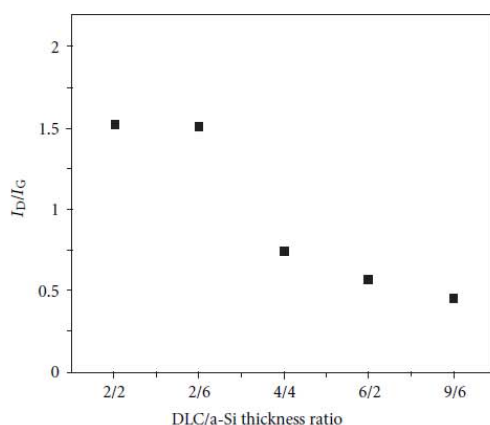


FIGURE 5: Plot of I_D/I_G ratio of the bilayer film as a function of DLC/a-Si thickness ratio. Decrease in the I_D/I_G ratio represents the increase in sp^3 contents of the films.

prepared from all types of DLC/a-Si thickness ratio are very close to the tetrahedral amorphous carbon (ta-C). Thickness of a-Si layer, a seed layer to improve the adhesion between DLC and substrate, barely affects the DLC formation and the sp^3 bonded. This information can be applied for developing DLC for bi- and multilayer protective coatings in which structural characteristics such as sp^3 content can be analyzed easily from the modified plot.

Acknowledgments

This work was supported by Industry/University Cooperative Research Center (I/UCRC) in HDD Advanced Manufacturing, Institute of Field roBOTics, King Mongkut's University of Technology Thonburi and National Electronics and Computer Technology Center, National Science and Technology Development Agency. It was also supported by KMUTT under the National Research University Project and Thailand Center of Excellence in Physics.

References

- [1] J. Robertson, "Ultrathin carbon coatings for magnetic storage technology," *Thin Solid Films*, vol. 383, no. 1-2, pp. 81-88, 2001.
- [2] J. Robertson, "Diamond-Like Amorphous carbon," *Materials Science and Engineering*, vol. 37, pp. 129-281, 2002.
- [3] F. X. Liu and Z. L. Wang, "Thickness dependence of the structure of diamond-like carbon films by Raman spectroscopy," *Surface and Coatings Technology*, vol. 203, no. 13, pp. 1829-1832, 2009.
- [4] J. J. Rha, S. C. Kwon, J. R. Cho, S. Yim, and N. Saka, "Creation of ultra-low friction and wear surfaces for micro-devices using carbon films," *Wear*, vol. 259, no. 1-6, pp. 765-770, 2005.
- [5] H. Kohira, V. Prabhakaran, and F. E. Talke, "Effect of air bearing design on wear of diamond-like carbon coated proximity recording sliders," *Tribology International*, vol. 33, no. 5, pp. 315-321, 2000.
- [6] N. Gopinathan, C. Robinson, and F. Ryan, "Characterization and properties of diamond-like carbon films for magnetic recording application," *Thin Solid Films*, vol. 355, pp. 401-405, 1999.
- [7] A. C. Ferrari and J. Robertson, "Interpretation of Raman spectra of disordered and amorphous carbon," *Physical Review B*, vol. 61, no. 20, pp. 14095-14107, 2000.
- [8] C. Weissmantel, K. Bewilogua, D. Dietrich et al., "Structure and properties of quasi-amorphous films prepared by ion beam techniques," *Thin Solid Films*, vol. 72, no. 1, pp. 19-31, 1980.
- [9] N. Savvides, "Optical constants and associated functions of metastable diamondlike amorphous carbon films in the energy range 0.5-7.3 eV," *Journal of Applied Physics*, vol. 59, no. 12, pp. 4133-4145, 1986.
- [10] M. S. Leu, S. Y. Chen, J. J. Chang, L. G. Chao, and W. Lin, "Diamond-like coatings prepared by the filtered cathodic arc technique for minting application," *Surface and Coatings Technology*, vol. 177-178, pp. 566-572, 2004.
- [11] J. Y. Shim, E. J. Chi, H. K. Baik, and S. M. Lee, "Structural, optical, and field emission properties of hydrogenated amorphous carbon films grown by helical resonator plasma enhanced chemical vapor deposition," *Japanese Journal of Applied Physics*, vol. 37, no. 2, pp. 440-444, 1998.
- [12] H. J. Scheibe, D. Drescher, B. Schultrich, M. Falz, G. Leonhardt, and R. Wilberg, "The laser-arc: a new industrial technology for effective deposition of hard amorphous carbon films," *Surface and Coatings Technology*, vol. 85, no. 3, pp. 209-214, 1996.
- [13] A. Grill, "Diamond-like carbon: state of the art," *Diamond and Related Materials*, vol. 8, no. 2-5, pp. 428-434, 1999.
- [14] M. V. Gradowski, A. C. Ferrari, R. Ohr et al., "Resonant Raman characterisation of ultra-thin nano-protective carbon layers

- for magnetic storage devices,” *Surface and Coatings Technology*, vol. 174–175, pp. 246–252, 2003.
- [15] F. X. Liu, K. L. Yao, and Z. L. Liu, “Substrate bias effect on structure of tetrahedral amorphous carbon films by Raman spectroscopy,” *Diamond and Related Materials*, vol. 16, no. 9, pp. 1746–1751, 2007.
 - [16] P. J. Fallon, V. S. Veerasamy, C. A. Davis et al., “Properties of filtered-ion-beam-deposited diamondlike carbon as a function of ion energy,” *Physical Review B*, vol. 48, no. 7, pp. 4777–4782, 1993.
 - [17] F. X. Liu, K. L. Yao, and Z. L. Liu, “Different substrate materials effect on structure of ta-C films by Raman spectroscopy for magnetic recording sliders,” *Journal of Non-Crystalline Solids*, vol. 353, no. 26, pp. 2545–2549, 2007.
 - [18] K. W. R. Gilkes, S. Prawer, K. W. Nugent et al., “Direct quantitative detection of the sp³ bonding in diamond-like carbon films using ultraviolet and visible Raman spectroscopy,” *Journal of Applied Physics*, vol. 87, no. 10, pp. 7283–7289, 2000.
 - [19] A. Grill, B. S. Meyerson, V. V. Patel, J. A. Reimer, and M. A. Petrich, “Inhomogeneous carbon bonding in hydrogenated amorphous carbon films,” *Journal of Applied Physics*, vol. 61, no. 8, pp. 2874–2877, 1987.

APPENDIX D

Effect of Surface Energy on the Growth of Diamond-like Carbon/Amorphous Silicon Films on Various Substrates

C. Srisang^{*1,2,3}, P. Asanithi¹, S. Limsuwan¹, A. Pokaipisit^{1,3} and P. Limsuwan^{*1,3}

¹Department of Physics, Faculty of Science, King Mongkut's University of Technology Thonburi, Bangkok 10140, Thailand

²Western Digital (Thailand) Company Limited, Ayuthaya 13160, Thailand.

³Thailand Center of Excellence in Physics, CHE, Ministry of Education, Bangkok 10400, Thailand.

Abstract

Diamond-like carbon/amorphous silicon bilayer films were deposited on SiO₂, Ge, and Ta₂O₅ substrates using a pulsed filtered cathodic arc (PFCA) system. Amorphous silicon (a-Si) layer was firstly deposited on three substrates using DC magnetron sputtering, then diamond-like carbon (DLC) film was deposited on a-Si layer via pulsed filtered cathodic arc. The thicknesses of a-Si layer and DLC film as monitored by *in-situ* ellipsometry during the film deposition were 7 and 10 nm, respectively. The surface energy of SiO₂, Ge and Ta₂O₅ substrates was determined by measuring the contact angle of water on these substrates. It was found that the contact angles of water on SiO₂, Ge and Ta₂O₅ substrates were 53°, 63° and 75°, respectively. This result indicates that SiO₂ has the highest surface energy while Ta₂O₅ has the lowest surface energy. The thickness of a-Si layer and DLC film was determined from the cross-section transmission electron microscopy (TEM) images. The thinnest a-Si layer of 5.64 nm was obtained from SiO₂ substrate which has the highest surface energy. The thickest a-Si layer of 6.97 nm was obtained from Ta₂O₅ corresponding to the lowest surface energy. This study shows that the thickness of the growth film strongly depends on the surface energy of the substrate. However, the DLC films deposited on each a-Si layer of three substrates have the same thickness approximately of 9.9 nm, because all of them were deposited on a-Si layers having the same surface energy.

Keywords: DLC film, Surface energy, Contact angle, Amorphous silicon

*Corresponding authors. Tel: +66 2872 5253, Fax: +66 2872 5254

E-mail address: opticslaser@yahoo.com

1. Introduction

The diamond-like carbon (DLC) film has many attractive properties, such as high hardness, high wear resistance, high corrosion resistance, low friction coefficient and chemical stability^[1-4]. In current hard disk drive technology, DLC films have been used as protective overcoat on the head and disk surfaces in magnetic storage devices^[5-7]. The DLC film behaves as a barrier to prevent the head and magnetic media against wear and corrosion^[7,8]. As the recording density continues to increase rapidly, the further reduction of the magnetic spacing between the head and disk is required and hence the thickness of DLC film must be reduced^[7,9]. In order to further increase the storage density up to 1 Tbit/in², it is desirable to reduce the magnetic spacing to less than 10 nm, so as to the DLC film with 1-2 nm thickness is needed^[6,10].

In the present magnetic storage industry, the thickness of ultra-thin DLC films has been reduced to ~2 nm with a maximum storage density of about 100 Gb/in²^[7]. In the industrial processing of ultra-thin DLC film, the *in-situ* ellipsometry was used for real-time process control of the film thickness. Tantalum pentaoxide (Ta₂O₅) wafer with a diameter of 2 inches was used as a substrate for film thickness monitoring due to high reflectivity surface. However, the real substrates used for the recording heads can be AlTiC, Al₂O₃, NiFe, Si and Ge. Therefore, it is doubtful that whether the growth rate of DLC film on each substrate is equal to that on the monitored Ta₂O₅ substrate.

In this work, SiO₂ and Ge together with Ta₂O₅ were used as substrates for studying the effect of substrate surface energy on the growth behavior of the deposited films. Amorphous silicon (a-Si) layer with a thickness of 7 nm was firstly sputtered on SiO₂, Ge and Ta₂O₅ substrates to improve the adhesion and strength of the DLC film. DLC film with a thickness of 10 nm was then deposited on the a-Si layer using a pulsed filtered cathodic arc (PFCA) system. It should be noted that SiO₂ was obtained from the growth of native oxide on Si substrate with a thickness of ~2 nm.

2. Experimental

2.1 Pulsed filtered cathodic arc system^[11]

The pulsed filtered cathodic arc (PFCA) system used in this work (Veeco, model Nexus DLC-X) is shown by a schematic diagram in Fig.1. The system consists of four vacuum chambers, including (i) load lock chamber, (ii) transfer chamber, (iii) pre-clean chamber and (iv) PFCA chamber. All chambers were attached together by isolation gate valve. Each has its own turbo molecular pump to evacuate the chamber individually. Ionization gauges were used to measure the pressure in all four chambers. Prior to the deposition processing of the DLC films, all chambers were evacuated to a base pressure of about 5.0×10^{-7} torr.

The transfer chamber was equipped with an automated robot arm system for transferring the substrate from load lock chamber to pre-clean and PFCA chambers. The pre-clean chamber was equipped with RF ion source, 16 inch in diameter, and DC magnetron sputtering source with a target of 4 inch in diameter. The ion source was used for pre-cleaning of the substrate whereas the DC magnetron source was used for the deposition of a-Si as a seed layer. The substrate with deposited silicon layer was then transferred to substrate fixture in the PFCA chamber by robot arm. The PFCA chamber was equipped with a cathodic arc for the deposition of DLC film.

The substrate fixtures in pre-clean and PFCA chambers are capable of tilt and rotation. Therefore, the a-Si seed layer and DLC film can be deposited onto the substrate at any required incident angle. Pre-clean and PFCA chambers were installed with a multi-wavelength ellipsometry (J.A. Woollam, M-2000) for *in situ* monitoring of the film thickness of a-Si layer and DLC film, respectively.

2.2 Films preparation

Three types of substrate used in the experiment were silicon dioxide (SiO_2), germanium (Ge), and tantalum pentaoxide (Ta_2O_5), where Ta_2O_5 was used as a film thickness monitoring. The dimension and thickness for each substrate were 1 cm \times 1 cm and 0.5 mm. The DLC/a-Si deposition process consists of three steps: (i) SiO_2 , Ge and Ta_2O_5 substrates were cleaned with low energy Ar^+ ion plasma etching for 60 seconds, (ii) a-Si layer was deposited on three substrates using DC magnetron with a power of 150 W and an argon gas flow rate of 40 sccm, and (iii) DLC layer was deposited on a-Si layer using a PFCA system with a pulse frequency of 1 Hz, arc voltage of 900 V and coil voltage of 850 V. The first two steps were carried out in pre-clean chamber while the third step was done in PFCA chamber. The film thickness was monitored using *in-situ* ellipsometry. In this work, the thicknesses of a-Si and DLC layers were set at 7 and 10 nm, respectively.

2.3 Characterization

2.3.1 Contact angle measurements

The surface energy of the substrate was analyzed with regard to contact angle measurement. It is well-known that wetting ability of liquid on a solid surface is controlled by atomic mechanisms occurring at the solid/liquid/vapor interface, depending upon the surface phenomenon between adsorbent and adsorbate, such as adsorption, desorption, diffusion and evaporation^[12-13]. The contact angle (ρ) can be used as a simple indicator for wetting ability of liquid on a solid surface, i.e. $\rho < 90^\circ$ and $\rho > 90^\circ$ determine wetting and non-wetting conditions, respectively. Therefore, prior to the deposition of a-Si and DLC films, the contact angles of water droplet on bare SiO_2 , Ge and Ta_2O_5 substrates were measured.

2.3.2 Surface morphology

The wetting ability as described above can generally be influenced by the surface roughness of the substrate, thus, all surface roughnesses of the substrate were examined using atomic force microscopy (AFM, Park Systems XE-150). The thickness of the growth a-Si and DLC films on SiO_2 , Ge and Ta_2O_5 substrates was investigated using transmission electron microscopy (TEM, Tecnai G² 20). Before carrying out the cross-section TEM image, each DLC/a-Si film was deposited with Cr. This Cr additional layer was used as a protective layer to prevent the passivation from ion bombardment during the sample preparation for cross-section TEM imaging using a focused ion beam (FIB) technique.

3. Results and discussion

For contact angle measurements, 1- μL water droplet was dropped at 5 different positions on the substrate surface at room temperature and 5 values of contact angle were obtained. The average values of contact angle of water droplet on SiO_2 , Ge and Ta_2O_5 substrates are given in Table 1. The typical photographs of 1- μL water droplet on SiO_2 , Ge and Ta_2O_5 substrates are shown in Figs. 2(a)-(c). As shown in Table 1 and Figs. 2(a)-(c), the contact angles of 1- μL water droplet on SiO_2 , Ge and Ta_2O_5 substrates are approximately 53° , 63° and 75° , respectively. The angle also gives information on the surface energy of the substrate. The relation between the contact angle and surface energy can be

discussed based on Young's equation and adhesive energy (the amount of energy required to separate two bodies). Here, the surface energy is the adhesive energy^[14].

When separating the bodies apart, one interface at body L/body S disappears, see Fig.3(a). Two new interfaces, body L/ambient and body S/ambient, arise. Therefore, the total energy change per unit surface area in such a process is

$$E_{adh} = \gamma_L + \gamma_S - \gamma_{LS} \quad (1)$$

where E_{adh} is adhesive energy, γ_L is liquid-vapor interfacial tension, γ_S is solid-vapor interfacial tension and γ_{LS} is liquid-solid interfacial tension.

If the body L is a liquid drop (Fig. 3(b)), and body S is a solid substrate, then the contact angle (θ) exhibited by the liquid drop at the surface of the substrate is determined by the Young's equation^[14].

$$\cos \theta = \frac{\gamma_S - \gamma_{LS}}{\gamma_L} \quad (2)$$

By combining Eq.(1) and Eq.(2), we obtain

$$E_{adh} = \gamma_L + \gamma_S - \gamma_{LS} = \gamma_L (1 + \cos \theta) \quad (3)$$

The typical values of the surface energy of water as a function of contact angle is given in Table 2. It is clearly observed that the lower the contact angle, the higher the surface energy of the solid surface. In present study, the contact angles of water droplet on SiO₂, Ge and Ta₂O₅ substrates are 53°, 63° and 75°, respectively. This result indicates that SiO₂ substrate has the highest surface energy while Ta₂O₅ substrate has the lowest surface energy. The schematics in Fig.2(d)-(g) show a-Si nuclei formed as droplet-like cluster on the substrate of different surface energies. This assumption is based on the general mechanism of thin film growth^[15, 16].

Fig. 4 shows the surface morphology of bare SiO₂, Ge and Ta₂O₅ substrates as investigated by AFM in tapping mode and a scanning area of 1 $\mu\text{m} \times 1 \mu\text{m}$. The root mean square (RMS) roughness of the three substrate surfaces obtained from Fig. 4 is given in Table 1. The RMS roughness of SiO₂, Ge and Ta₂O₅ was found to be 0.31, 2.83 and 0.33 nm, respectively. However, the results are not correlated with the contact angle values.

The growth of DLC/a-Si films on SiO₂, Ge and Ta₂O₅ substrates was further investigated using TEM. Fig. 5 shows cross-section bright-field TEM images of DLC/a-Si bilayer film deposited on SiO₂, Ge and Ta₂O₅ substrates, respectively. The thickness of a-Si and DLC films was determined from the original TEM images at 10 different positions. The average thickness of a-Si and DLC films on SiO₂, Ge and Ta₂O₅ substrates is given in Table 3. It was found that the thicknesses of a-Si layers on SiO₂, Ge and Ta₂O₅ are 5.64, 6.30 and 6.97 nm, respectively, whereas those of DLC layers on the a-Si layers are the same. To have further understanding on these phenomena, the effect of the adsorbent surface energy on the film-growth mechanism of a-Si layer and DLC film is discussed.

For the a-Si layer, the difference in thickness may be resulted from the wetting ability of a-Si liquid on the substrate which is a function of the surface energy of the solid/liquid/gas interface. The early stage of a-Si film growing is an important step that affects the overall thickness of a-Si layer. This early stage is called nucleation stage (formation of film nucleus). At this nucleation stage of the a-Si film growing, Si atoms or molecules approach and accommodate on the substrate surface. The migration and aggregation of Si molecules along the substrate surface begin to form 2D clusters (nanocluster) resembling liquid droplets (or island) on the substrate^[15]. The contact angle of liquid droplet at the nucleation stage is dependent on the surface energy of the substrate. The higher contact angle of the liquid droplet offers thicker film as shown in Figs.2(c) and (e). The nuclei continue to grow as a random network until they coalesce^[16] and the substrate surface is finally covered with a-Si layer, called an initial layer. Then, more Si molecules are deposited on this initial layer until the a-Si layer becomes thicker.

The difference in the average thickness of a-Si layer on the substrates may be related to the difference in surface energy of the substrate as previously mentioned. As shown in Fig. 2, the contact angle measurement was employed as a simple methodology to obtain information on the surface energy of the substrate. The lower contact angle indicates that the substrate has higher surface energy. The contact angles of water droplet on SiO₂, Ge, and Ta₂O₅ substrates are approximately 53°, 63° and 75°, respectively. It is seen in Table 3 that the thickness of a-Si layer is inversely proportional to the surface energy of the substrate. The thinnest a-Si layer, 5.64 nm, was obtained from SiO₂ substrate which has the highest surface energy. The thickest a-Si layer, 6.97 nm, was obtained from Ta₂O₅ substrate corresponding to the lowest surface energy. The Ge substrate, having the surface energy in the range between those of SiO₂ and Ta₂O₅ substrates, offered the a-Si layer of 6.30 nm.

The lowest surface energy of Ta₂O₅ substrate leads to the thickest a-Si layer because it can build up more globular droplet as shown in Figs. 2(c) and (e). It is this globular droplet that affects the

thickness of the a-Si layer. In contrast, the highest surface energy of SiO₂ substrate induces almost flat droplet, see Figs. 2(a) and (d) and, then, the flat droplet leads to the thinnest a-Si layer of 5.64 nm, as shown by cross-section bright-field TEM images in Fig. 5.

The DLC film thickness on the three substrates, however, was approximately the same with 9.9 nm thick, as shown in Table 3. This is due to the DLC films grown on the a-Si layers of three substrates with equivalent surface energy of a-Si layers. As previous discussion on the early stage of the growth of a-Si layer, the growth of DLC film is also similar to that of a-Si layer. The wetting ability of DLC molecules on the a-Si layer from each substrate was the same. Thus, the thicknesses of the DLC films from different substrates was similar. Fig. 6 shows three-dimensional images of DLC films on different substrates obtained from atomic force microscopy (AFM, 1 μ m x 1 μ m). The values of the RMS roughness of the DLC films on SiO₂, Ge and Ta₂O₅ substrates are 0.17, 0.30 and 0.31 nm, respectively. The little difference in the RMS roughness of the DLC films may be due to the difference in the initial roughness values of the bare substrates.

4. Conclusions

The surface energy of the substrate could play an important role on the growth of a-Si layer. The thickness of a-Si layer deposited on the substrate can be addressed by the wetting ability of the substrate surface at the early stage of the film formation. The wetting ability is inversely proportional to the surface energy. In this work, the lowest surface energy of Ta₂O₅ substrate yielded the thickest a-Si layer since it can build up more globular droplet of a-Si molecules at the initial step of the film growth. However, the highest surface energy of SiO₂ substrate induced almost a flat droplet of a-Si molecules, consequently leading to form the thinnest a-Si layer. Unlike the a-Si layer, the DLC films deposited on a-Si layers of the three substrates have the same thicknesses approximately of 9.9 nm, because all of them were deposited on a-Si layer-coated substrates having the same surface energy.

Acknowledgment

This work was supported by Industry/ University Cooperative Research Center (I/UCRC) in HDD Advanced Manufacturing, Institute of Field roBOTics, King Mongkut's University of Technology Thonburi and National Electronics and Computer Technology Center, National Science and Technology Development Agency. This work was partially supported by Thailand Center of Excellence in Physics (ThEP) and King Mongkut's University of Technology Thonburi under The National Research University Project.

References

1. Xiang, Y., Cheng-biao, W., Yang, L., De-yang, Y., A Study of Hard Diamond-Like Carbon Films in Mid-Frequency Dual-Magnetron Sputtering, *Diam. Relat. Mater.* 15 (2006) 1223-1227.
2. Zhang, S., Fu, Y., Du, H., Zeng, X.T., Liu, Y.C., Magnetron Sputtering of Nanocomposite (Ti, Cr)/CN/DLC Coatings, *Surf. Coat. Technol.* 162 (2002) 42-48.
3. Paik, N., Raman and XPS Studies of DLC Films Prepared by a Magnetron Sputter-Type Negative Ion Source, *Surf. Coat. Technol.* 200 (2005) 2170-2174.
4. Hamdy, A.S., Electrochemical Behavior of Diamond-Like-Carbon Coatings Deposited on AlTiC (Al₂O₃+TiC) Ceramic Composite Substrate in HCL Solution, *Electrochimica Acta.* 56 (2011) 1554-1562.
5. Casiraghi, C., Robertson, J., Ferrari, A. C., Diamond-Like Carbon for Data and Beer Storage, *Mater. Today.* 10 (2007) 44-53.
6. Ferrari, A. C., Diamond-Like Carbon for Magnetic Storage Disks, *Surf. Coat. Technol.* 180-181 (2004) 190-206.
7. Zhong, M., Zhang, C., Luo, J., Lu, X., The Protective Properties of Ultra-Thin Diamond Like Carbon Films for High Density Magnetic Storage Devices, *Appl. Surf. Sci.* 256 (2009) 322-328.
8. Casiraghi, C., Ferrari, A.C., Ohr, R., Chu, D., Robertson, J., Surface Properties of Ultra-Thin Tetrahedral Amorphous Carbon Films for Magnetic Storage Technology, *Diam. Relat. Mater.* 13 (2004) 1416-1421.
9. Bernhard, P., Ziethen, Ch., Ohr, R., Hilgers H., Schönhense, G., Investigations of the Corrosion Protection of Ultrathin a-C and a-C:N Overcoats for Magnetic Storage Devies, *Surf. Coat. Technol.* 180-181 (2004) 621-626.
10. Casiraghi, C., Ferrari, A.C., Robertson, J., Ohr, R., Gradowski, M.v., Schneider, D., Hilgers, H., Ultra-Thin Carbon Layer for High Density Magnetic Storage Devices, *Diam. Relat. Mater.* 13 (2004) 1480-1485.

11. Srisang, C., Asanithi, P., Siangchaew, K., Pokaipisit, A., Limsuwan, P., Characterization of SiC in DLC/a-Si films prepared by pulsed filtered cathodic arc using Raman spectroscopy and XPS, *Appl. Surf. Sci.*, 258 (2012) 5605-5609.
12. Wagner, R.S., Ellis, W.C., Vapor-Liquid-Solid Mechanism of Single Crystal Growth, *Appl. Phys. Lett.*, 4 (1964) 89-90.
13. Baranauskas, V., Tosin, M.C., Peterlevitz, A.C., Ceragioli, H., Durrant, S.F., Enhancement of Diamond Nucleation Using the Solid-Liquid-Gas Interface Energy, *J. Appl. Phys.*, 88 (2000) 1650-1654.
14. Good, R. J. Contact angle, wetting, and adhesion: a critical review. *J. Adhesion Sci. Technol.* 6 (12) (1992) 1269-1302.
15. Ohring M., *Materials Science of Thin Films*, Academic Press, San Diego, Calif, USA, 2nd edition, 2002
16. Asanithi, P., Chaiyakun, S., Limsuwan, P., Growth of silver nanoparticles by DC magnetron sputtering, *J. of Nanomaterials*, 2012, 2012, 1-8.

Table Captions

- Table 1 Contact angle of water droplet (1 μ L) and root mean square (RMS) roughness of the bare substrates. The average contact angle from each substrate was measured from 5 different positions on the substrate surface at room temperature.
- Table 2 Relation between the surface energy and contact angle of water at 25°C, the surface tension of water, $\gamma_L = 71.97$ mN/m.
- Table 3 Average thickness of a-Si layer and DLC film, and root mean square (RMS) roughness of DLC film on different substrates. The thickness of a-Si and DLC films was averaged from 10 positions in TEM image.

Figure Captions

- Figure 1 Schematic diagram of pulsed filtered cathodic arc (PFCA) system.
- Figure 2 Contact angle of water droplet (1 μ L) on different substrates: (a) SiO₂ (53°), (b) Ge (63°) and (c) Ta₂O₅ (75°). Schematics in (d)-(g) show that a-Si may form a droplet-like cluster on the substrate of different surface energies. Surface energy affects the shape and height of droplets.
- Figure 3 (a) One interface (γ_{LS}) at body L/body S (left) and two new interfaces (γ_L and γ_S) for body L/ambient and body S/ambient (right), and (b) the body L is a liquid drop, then the contact angle (θ) is exhibited by the liquid drop.
- Figure 4 Surface morphology of bare substrates: (a) SiO₂, (b) Ge and (c) Ta₂O₅.
- Figure 5 Cross-section bright-field TEM images of a-Si and DLC films deposited on different substrates: (a) SiO₂, (b) Ge and (c) Ta₂O₅. Note that the thickness of SiO₂ layer is only 2 nm due to the growth of native oxide on Si substrate.
- Figure 6 Surface topography of DLC film on different substrates: (a) SiO₂, (b) Ge, and (c) Ta₂O₅. The data were obtained from AFM measurements.

Table 1 Contact angle of water droplet (1 μ L) and root mean square (RMS) roughness of the bare substrates. The average contact angle from each substrate was measured from 5 different positions on the substrate surface at room temperature.

Substrate	Contact angle (degree)	RMS roughness, (nm)
SiO ₂	52.92 \pm 0.89	0.31
Ge	63.02 \pm 1.52	2.83
Ta ₂ O ₅	75.30 \pm 1.23	0.33

Table 2 Relation between the surface energy and contact angle of water at 25°C, the surface tension of water, $\gamma_L = 71.97$ mN/m.


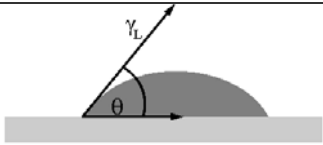
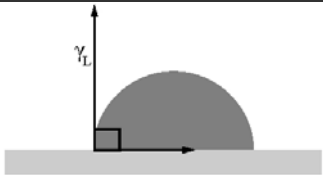
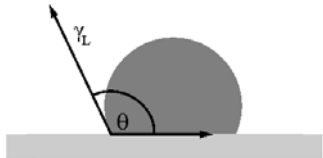

Contact angle (Degree)		$E_{adh} = \gamma_L (1 + \cos\theta)$ (mN/m)	Degree of wetting
0		$E_{adh} = 2 \gamma_L = 143.94$	Perfect wetting
45		$E_{adh} = 1.71 \gamma_L = 123.07$	High wettability
90		$E_{adh} = \gamma_L = 71.97$	Low wettability
120		$E_{adh} = 0.5 \gamma_L = 35.99$	Low wettability
180		$E_{adh} = 0$	Perfectly non-wetting

Table 3 Average thickness of a-Si layer and DLC film, and root mean square (RMS) roughness of DLC film on different substrates. The thickness of a-Si and DLC films was averaged from 10 positions in TEM image.

Substrate	Average film thickness (nm)		RMS roughness, (nm)
	a-Si	DLC	
SiO ₂	5.64 ± 0.14	9.91 ± 0.15	0.17
Ge	6.30 ± 0.16	9.96 ± 0.19	0.30
Ta ₂ O ₅	6.97 ± 0.17	10.02 ± 0.30	0.31

P. Limsuwan *et al.*

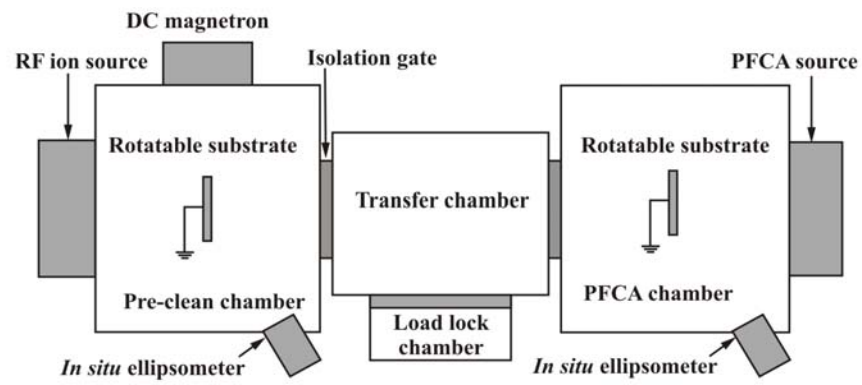


Figure 1.

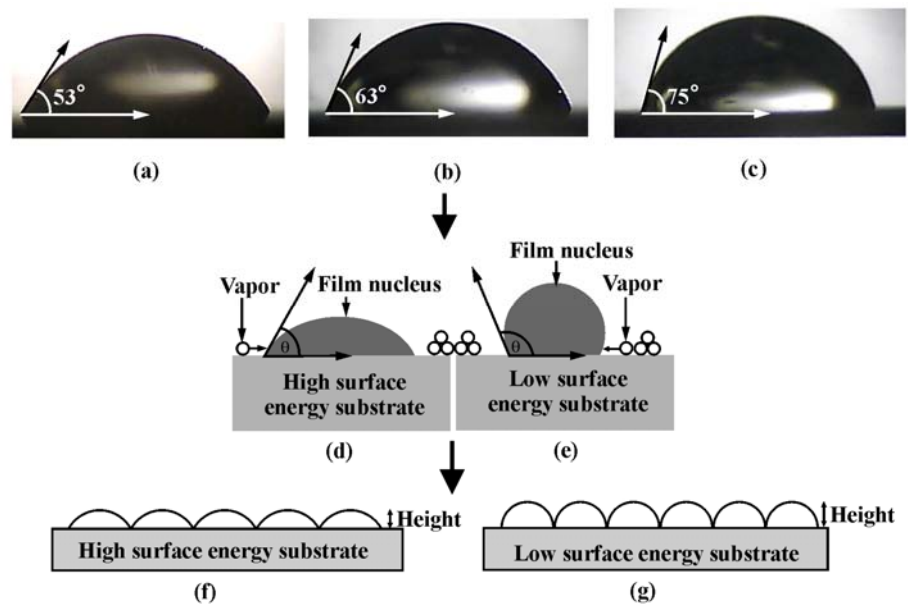


Figure 2

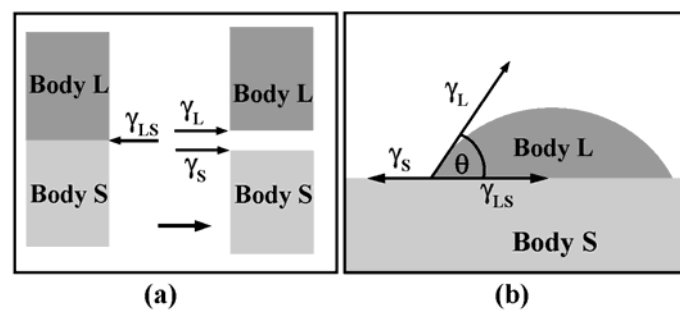


Figure 3

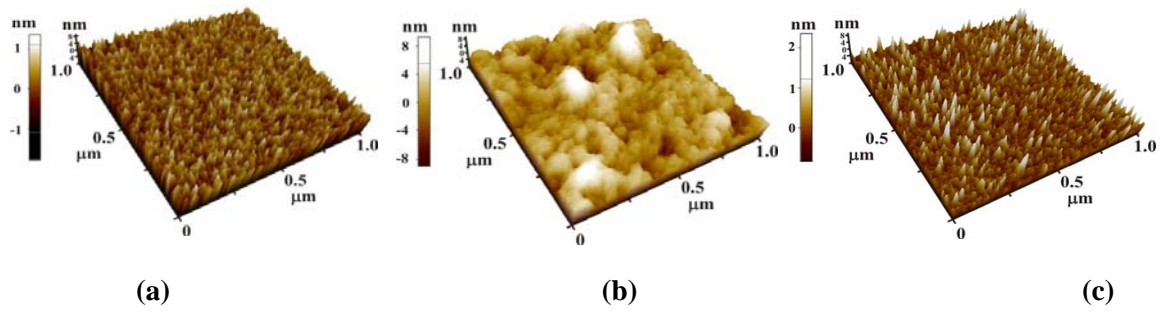


Figure 4

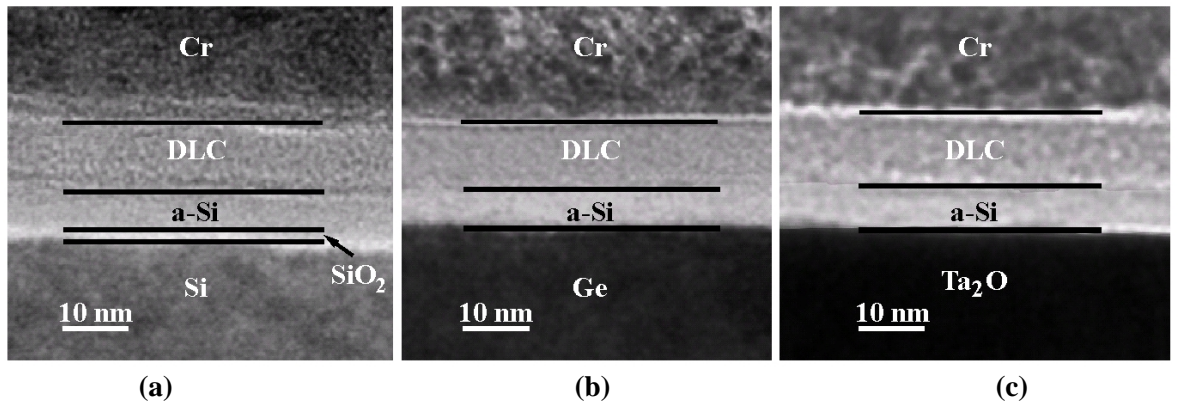


Figure 5

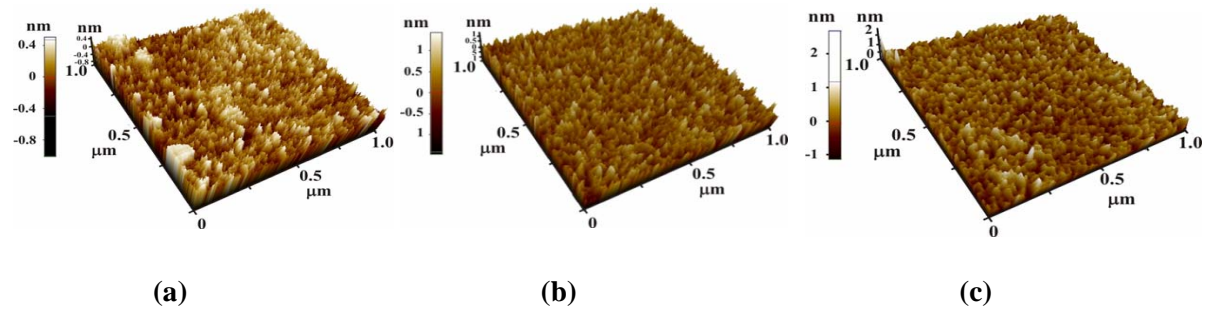


Figure 6

APPENDIX E

Formation of SiC in DLC/a-Si films as characterized by Raman spectroscopy and XPS

C Srisang^{1,2,3,a}, P Asanithi¹, K Siangchaew², A Pokaipisit^{1,3,b} and P Limsuwan^{1,3}

¹ Department of Physics, Faculty of Science, King Mongkut's University of Technology Thonburi, Bangkok, 10140, Thailand

² Western Digital (Thailand) Company Limited, Ayuthaya, 13160, Thailand

³ Thailand Center of Excellence in Physics, CHE, Ministry of Education, Bangkok 10400, Thailand

E-mail: ^aJirawat.Srisung@wdc.com, ^bpokaipisit@gmail.com

Abstract. Bilayer DLC/a-Si films was deposited on germanium substrate. a-Si films was initially deposited as a seed layer on the substrate using DC magnetron sputtering. DLC films was then deposited on the a-Si layer via a pulsed filtered cathodic arc (PFCA) system. *In situ* ellipsometry was used to monitor growth in thickness of a-Si and DLC films, allowing a good control over growth conditions. The thickness of DLC and a-Si layers were 9 nm and 6 nm, respectively. In this work, the interface of a-Si and DLC layers was investigated by Raman spectroscopy and X-ray photoelectron spectroscopy (XPS). It was found that the SiC layer was formed at the interface of a-Si and DLC layers.

1. Introduction

Diamond like carbon (DLC) consists of an amorphous form of the carbon containing both graphitic type bonding (sp^2) and diamond type tetrahedral bonding (sp^3) [1]. The properties of this non-crystalline material cover a wide range and are intermediate between the properties of diamond, graphite, and hydrocarbon polymers [2]. The properties depend on the experimental parameters. Under appropriate deposition condition, chemically inert and optically transparent films can be prepared [3]. As the hardness of DLC films approaches that of diamond, at present, it has been widely used as a protective layer on magnetic recording head and disk media [3, 4]. DLC films are also finding applications as corrosion resistant coating, anti reflection and scratch proof coating on germanium and silicon optics [5]. Another important application of these coatings is for bearing because of their low sliding friction on the metals.

DLC films can be prepared by various techniques, i.e. ion beam assisted deposition [6], sputtering [7], filtered cathodic vacuum arc [8], plasma-assisted chemical vapor deposition [9], and pulsed laser deposition [10]. It was reported that structure and properties of DLC films can be controlled by substrate bias [11, 12]. An important problem appears in DLC film deposition is the ability to control physical properties of the film over a substrate. Different types of substrate or substrates of different roughness may provide different physical properties of the film, e.g. surface roughness [13]. Moreover, the problem of low adherence on the substrate is also significant. The interface layer between the substrate and DLC films may play an important role. Castillo *et al.* improved the adherence of DLC films using amorphous hydrogenated carbon (a-C:H) and titanium nitride (TiN) as interface layer between DLC films and silicon substrate [14].

In current hard disk drive technology, ultra-thin DLC films have been used for coating on both disks and recording heads. However, prior to DLC coating a thin amorphous silicon (a-Si) layer is pre-coated on the substrate to increase the adhesion between the substrate and DLC films.

In this study, a-Si with a thickness of 6 nm was coated on germanium (Ge) substrate as a seed layer. Then, DLC films with a thickness of 9 nm was coated on a-Si film. The formation of SiC at the DLC/a-Si interface was investigated using Raman spectroscopy and X-ray photoelectron spectroscopy.

2. Experimental details

2.1. Pulsed filtered cathodic arc system

The pulsed filtered cathodic arc (PFCA) system used in this work (Veeco, model Nexus DLC-X) is shown by a schematic diagram in Figure 1. The system consists of four vacuum chambers, i.e. load lock chamber, transfer chamber, pre-clean chamber, and PFCA chamber. All chambers were attached together by isolation gate valve. Each has its own turbo molecular pump to evacuate the chamber individually. Ionization gauges were used to measure the pressure in all four chambers. Prior to the deposition processing of the DLC films, all chambers were evacuated to a base pressure of about 5.0×10^{-7} torr. The transfer chamber was equipped with an automated robot arm system for transferring the substrate from load lock chamber to pre-clean and PFCA chambers.

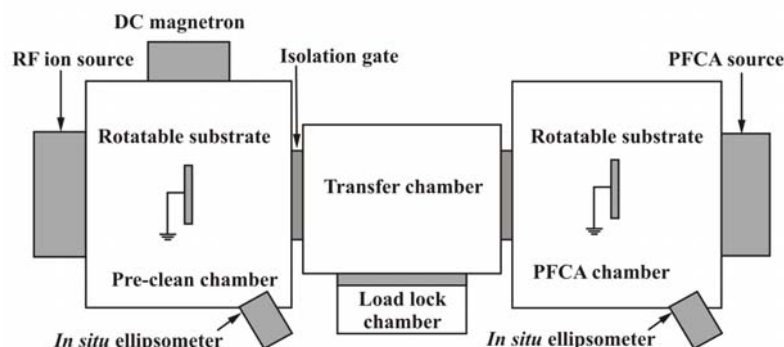


Figure 1. Schematic diagram of PFCA system.

The pre-clean chamber was equipped with radio frequency (RF) ion source, 16 inch in diameter, and DC magnetron sputtering source with a target of 4 inch in diameter. The ion source was used for pre-cleaning of the substrate whereas the DC magnetron source was used for the deposition of a-Si as a seed layer. The substrate with deposited silicon layer was then transferred to substrate fixture in the PFCA chamber by robot arm. The PFCA chamber was equipped with a cathodic arc for the deposition of DLC films.

The substrate fixtures in pre-clean and PFCA chambers are capable of tilt and rotation. Therefore, the a-Si seed layer and DLC films can be deposited onto the substrate at any required incident angle. Pre-clean and PFCA chambers were installed with a multi-wavelength ellipsometry (J.A. Woollam, M-2000) for *in situ* monitoring of the film thickness of a-Si layer and DLC films, respectively. Figure 2 shows a schematic diagram of PFCA chamber and cathodic arc source.

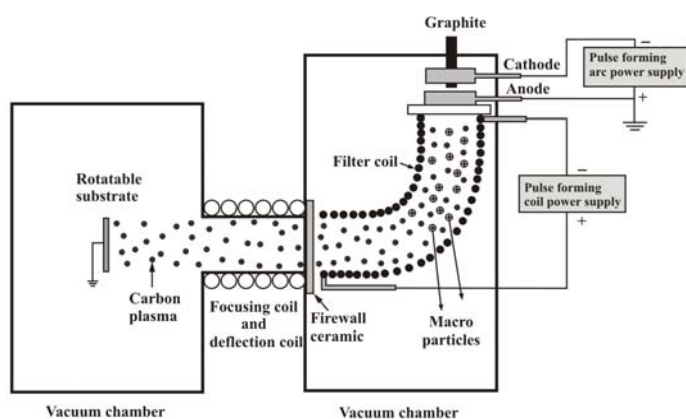


Figure 2. Schematic diagram of PFCA chamber and cathodic arc source.

The cathodic arc source includes a high purity graphite cathode of 0.25 inch in diameter and 8 inch in length (99.999% purity), obtained from Poco Graphite. The arc power supply is operated in pulsed mode. The positive potential of power supply is connected with anode and ground. The voltage between anode and cathode, called arc voltage, can be varied from 0-1000 V with pulse frequency of 1-5 Hz. Since the distance between anode and graphite cathode is about 2 mm, it is high enough to create current discharge between anode and cathode. Then, graphite is vaporized at the cathode. All charge particles are fed into a curved 90 degree filter coil. Electrons are moved in spiral along magnetic field generated by filter coil, and ions will be guided due to they are charge particles. In order to improve the film thickness uniformity, a coil operates as a magnetic lens to focus or defocus the plasma beam. A deflection coil is used to raster the beam before striking the substrate. The macro particles move in strange trajectory so they may either leave the filter through openings gap between the turns of the coil or stick to the turns. Thus, unwanted macro particles and neutral atoms are filtered out and coating species reaching the substrate are pure carbon plasma.

2.2. Films preparation

DLC films were deposited using the PFCA deposition method. Crystalline n-type Ge wafers with (100) orientation, and a dimension of 1 cm × 1 cm with a thickness of 0.5 mm were used as substrates.

The DLC deposition process consists of three steps: (1) the substrate was cleaned with low energy Ar^+ ion plasma etching at an incident angle of 60° with respect to substrate, for 60 seconds, (2) a-Si seed layer was deposited on the cleaned Ge substrate at an incident angle of 44° with respect to substrate, using DC magnetron with a power of 150 W and argon gas flow rate of 40 sccm, and (3) DLC layer was deposited at the normal incident angle with respect to substrate using PFCA with a pulse frequency of 1 Hz, arc voltage of 950 V and coil voltage of 900 V. The first two steps were carried out in pre-clean chamber while the third step was done in PFCA chamber. The film thickness was monitored using *in situ* ellipsometry. Figure 3 shows illustration of deposited films on Ge substrate.

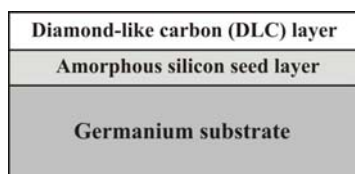


Figure 3. The layers of DLC films and a-Si layer on Ge substrate.

2.3. Characterization

Raman measurements were performed using Renishaw inViaReflex Raman Spectrometer with an excitation wavelength of 514 nm from Ar^+ ion gas laser. The laser output is 20 mW and the objective lens is 50x. The incident power on the sample is approximately 4 mW. The scan range was from 400 to 1900 cm^{-1} .

The XPS depth profiles were recorded by PHI Quantera SXM scanning X-ray using AlK_α X-ray source with a spot size of 200 μm . To obtain the depth profile, the DLC/a-Si (9/6 nm) film was etched using ion bombardment from an ion gun of 1 kV for acquiring the XPS spectrum information. Furthermore, the Shirley background type was used for XPS measurements.

3. Results and Discussion

Raman spectroscopy was used to investigate the vibrational modes of carbon and silicon atoms due to chemical bonding, especially in SiC, in the DLC/a-Si film. The longitudinal optical (LO) and the transversal optical (TO) phonon modes were observed at 796 cm^{-1} and 972 cm^{-1} , respectively, as shown in Figure 4.

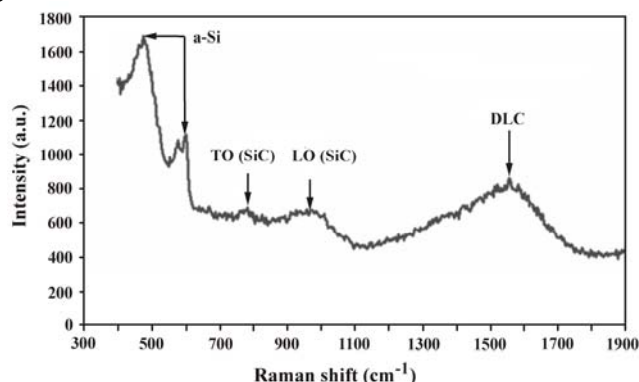


Figure 4. Raman spectra of coated DLC/a-Si films with a thickness of 9/6 nm.

The Raman shifts located at these positions are in agreement with those reported for 3C-SiC (β -SiC) [15]. The prominent peak at 480 cm^{-1} is related to the vibrational mode of a-Si since it was used as a seed layer for depositing the DLC films [16]. However, no peak from crystalline silicon at 520 cm^{-1} is observed. This suggests that during the deposition of a-Si layer on the Ge substrate there is probably no crystalline silicon formation. In the higher wavenumber, the wide band in the 1100-1800 cm^{-1} region is related to the vibrational modes of DLC graphitic characteristics, generally consisting of G and D bands.

Table 1. XPS binding energy of different bonds.

Bond	Binging energy (eV)
C-C	284 - 284.5
C-Si (C 1s)	282.3 - 283.7
Si-C (Si 2p)	99.8 - 101.3
Si-Si	99.2 - 99.6

Table 1 shows XPS binding energy after the resolved components in the DLC/a-Si film. The higher-energy range of 284-284.5 eV was assigned to the bonding of carbon atoms in the DLC films. The C 1s and Si 2p configurations, corresponding to the bonding between carbon and silicon atoms in SiC at the DLC and a-Si interface, are in the ranges of 282.3-283.7 eV and 99.8-101.3 eV, respectively [17]. The lowest-energy one in the range of 99.2-99.6 eV corresponds to the bonding of silicon atoms in a-Si layer.

In addition, the XPS sputter depth profile was also used to have further quantitative information on the SiC formation at the DLC/a-Si interface. The DLC/a-Si (9/6 nm) film was etched using ion bombardment for acquiring the XPS spectrum information. The actual depth for each XPS analysis depends upon the etching rate (sputter time) and the material being etched at any given depth.

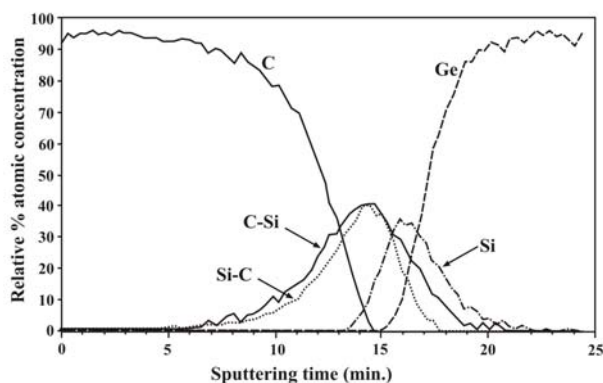


Figure 5. The XPS depth profile of DLC/a-Si films with a thickness of 9/6 nm on Ge substrate.

Figure 5 shows five major spectra of depth profile ranging from DLC films (top layer), SiC (C 1s and Si 2p) at the DLC and a-Si interface, a-Si layer, and Ge substrate. At the sputter time of less than 5 min, the depth profile represents the high percentage of DLC films of more than 90%. The DLC percentage gradually decreases for longer sputter time and becomes 0% at 15 min. At this time, the spectrum corresponding to a-Si layer is initially appeared and reaches the maximum content of 38% at 16 min of sputter time. The peaks obtained from the bonding between carbon and silicon atoms in the C 1s (C-Si) and the Si 2p (Si-C) locating in between those of DLC and a-Si films, are clearly observed as a result of the SiC formation. They reach the maximum contents of 41%. The last spectrum profile indicates the Ge substrate. From Figure 5, the thickness of SiC layer can be estimated and it was found to be approximately 2.8 nm.

4. Conclusions

We presented that there is the formation of SiC layer during the deposition of DLC/a-Si thin film. The LO and the TO phonon modes of SiC were observed at the Raman peaks of 796 cm^{-1} and 972 cm^{-1} , respectively. The result indicates that the SiC occurred between the DLC and a-Si interface is the 3C-SiC. The results were also confirmed using XPS binding energy and XPS depth profile analysis. There are two possible bonding configurations of carbon and silicon atoms at the interface, including the C 1s and the Si 2p which are in the ranges of 282.3-283.7 eV and 99.8-101.3 eV, respectively.

Acknowledgment

This work was supported by Industry/University Cooperative Research Center (I/UCRC) in HDD Advanced Manufacturing, Institute of Field roBOTics, King Mongkut's University of Technology Thonburi and National Electronics and Computer Technology Center, National Science and Technology Development Agency. This work was partially supported by Thailand Center of Excellence in Physics (ThEP) and King Mongkut's University of Technology Thonburi under The National Research University Project.

Reference

1. Gradowski M V, Ferrari A C, Ohr R, Jacoby B, Hilgers H, Schneider H H and Adrian H 2003 *Surf. Coat. Technol.* **174-175** 246
2. Robertson J 2002 *Mater. Sci. Eng. R* **37** 129
3. Kim Y T, Cho S M, Choi W S, Hong B and Yoon D H 2003 *Surf. Coat. Technol.* **169-170** 291
4. Liu F X and Wang Z L 2009 *Surf. Coat. Technol.* **203** 1829
5. Patil D S, Ramachandran K, Venkatramani N, Pandey M and Cunha R D 2000 *Pramana J. Phys.* **55** 933
6. Weissmantel C, Bewilogua K, Dietrich D, Erler H J, Hinneberg H J, Klose S, Nowick W and Reisse G 1980 *Thin Solid Films* **72** 19
7. Savvides N 1986 *J. Appl. Phys.* **59** 4133
8. Xu S, Tay B K, Tan H S, Zhong Li, Tu Y Q, Silva S R P and Milne W I 1996 *J. Appl. Phys.* **79** 7234
9. Shim J Y, Chi E J, Baik H K and Lee S M 1998 *Jpn. J. Appl. Phys.* **37** 440
10. Scheibe H S, Drescher D, Schultrich B, Falz M, Leonhardt G and Wilberg R 1996 *Surf. Coat. Technol.* **85** 209
11. Zhang W, Tanaka A, Wazumi K and Koga Y 2002 *Diam. Rel. Mater.* **11** 1837
12. Sheeja D, Tay B K, Lau S P and Shi Xu 2001 *Wear* **249** 433
13. Zhong M, Zhang C and Luo J 2008 *Appl. Surf. Sci.* **254** 6742
14. Castillo H A, Parra E R and Arango P J 2011 *Appl. Surf. Sci.* **257** 2665
15. Lee C J, Pezzotti G, Okui Y and Nishino S 2004 *Appl Surf Sci* **228** 10
16. Veres M, Koós M, Tóth S, Füle M, Pócsik I, Tóth A, Mohai M and Bertóti I 2005 *Diam. Rel. Mater.* **14** 1051
17. Cho W, Oh Y, Kim C, Osada M, Kakihana M, Lim D and Cheong D 1999 *J. Alloys Comp.* **285** 255